BIOCHEMISTRY
including biophysical chemistry & molecular biology

Article

pubs.acs.org/biochemistry

Terms of Use

Characterization of THB1, a *Chlamydomonas reinhardtii* Truncated Hemoglobin: Linkage to Nitrogen Metabolism and Identification of Lysine as the Distal Heme Ligand

Eric A. Johnson,[†] Selena L. Rice,[†] Matthew R. Preimesberger,[†] Dillon B. Nye,[†] Lukas Gilevicius,[†] Belinda B. Wenke,[†] Jason M. Brown,[‡] George B. Witman,*[,‡] and Juliette T. J. Lecomte*[,†]

[†]Department of Biophysics, Johns Hopkins University, Baltimore, Maryland 21218, United States

[‡]Department of Cell and Developmental Biology, University of Massachusetts Medical School, Worcester, Massachusetts 01655, United States

Supporting Information

ABSTRACT: The nuclear genome of the model organism *Chlamydomonas reinhardtii* contains genes for a dozen hemoglobins of the truncated lineage. Of those, *THB1* is known to be expressed, but the product and its function have not yet been characterized. We present mutagenesis, optical, and nuclear magnetic resonance data for the recombinant protein and show that at pH near neutral in the absence of added ligand, THB1 coordinates the heme iron with the canonical proximal histidine and a distal lysine. In the cyanomet state, THB1 is structurally similar to other known truncated hemoglobins, particularly the heme domain of *Chlamydomonas eugametos* LI637, a light-induced chloroplastic hemoglobin. Recombinant THB1 is capable of binding nitric oxide ($NO^{\bullet}$) in either the ferric or ferrous state and has efficient $NO^{\bullet}$ dioxygenase activity. By using different *C. reinhardtii* strains and growth conditions, we demonstrate that the expression of *THB1* is under the control of the *NIT2* regulatory gene and that the hemoglobin is linked to the nitrogen assimilation pathway.

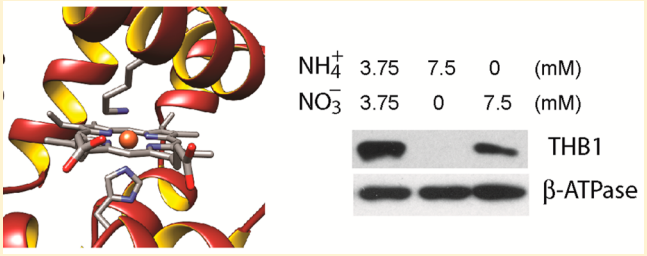

In 1992, Potts and co-workers[1] discovered in the cyanobacterium *Nostoc commune* a gene encoding a product resembling protozoan and mammalian myoglobins. It was remarkable that a protein commonly associated with dioxygen transport was found in cyanobacteria and intriguing that the gene was located within a nitrogen fixation operon. Subsequent investigations have provided evidence that *N. commune* "cyanoglobin" belongs to a distinct and well-represented lineage of the hemoglobin (Hb) superfamily,[2] which has been given the general name of truncated hemoglobins (TrHbs) in reference to their primary structures containing ~30 fewer amino acids than myoglobin (Mb). *N. commune* cyanoglobin is thought to be involved in dioxygen scavenging, presumably to protect the nitrogenase from oxidative damage.[3]

Shortly after the discovery of cyanoglobin, two light-induced TrHb genes, *LI410* and *LI637*, were found in the unicellular photosynthetic eukaryotic alga *Chlamydomonas eugametos* (*moewusii*).[4] Crystallization and subsequent structure determination of the globin domain of the *LI637* gene product (hereafter CtrHb) provided the first glimpse of a TrHb fold.[5] The heme group is buried in the protein, which adopts a two-on-two helical topology resulting from the shortened sequence. LI637, a protein targeted to the chloroplast, was one of the first TrHbs to be studied *in vivo*. Protection against oxidative damage was also proposed as a function for this Hb.[6]

Genes encoding proteins containing one or more Hb domains are present in virtually all forms of life and occur in three distinct lineages, including the TrHb family.[7] Recent genome analyses show a preponderance of TrHbs in cyanobacteria and green algae.[8] The phylogenetic data support the rise of TrHbs soon after the appearance of life on this planet, emerging perhaps 3 billion years ago.[7,9] During this early phase of life on Earth, atmospheric dioxygen levels were low (10^{-6} atm). Elevation of the dioxygen level resulted from subsequent geological upheaval and the evolution of photosynthesis roughly 2 billion years ago.[10,11] Given that the TrHb scaffold was formed long before the development of our current aerobic environment, an attractive original role for these proteins is dioxygen detoxification, as put forth for the modern *N. commune* and *C. eugametos* proteins.

The search for globin physiological functions in unicellular photosynthetic organisms is further guided by the observation that many Hbs (including members of the TrHb family) are capable of reacting with nitrogen−oxygen compounds such as nitric oxide ($NO^{\bullet}$),[12,13] nitrite, and peroxynitrite.[14] The reactions include oxidation, e.g., generation of nitrate from nitric oxide by oxy Hb; reduction, e.g., formation of nitric oxide

Received: April 29, 2014
Revised: June 23, 2014
Published: June 25, 2014

 © 2014 American Chemical Society dx.doi.org/10.1021/bi5005206 | *Biochemistry* 2014, 53, 4573−4589

from nitrite by deoxy Hb; and isomerization, e.g., conversion of peroxynitrite to nitrate by ferric (met) Hb, each process depending on the redox and ligation state of the protein. Such chemical versatility can be attained by alterations of the heme environment without disruption of the fold. Reactive nitrogen species (RNS) are present in and around photosynthetic algae and cyanobacteria as products of enzymes involved in nitrite or nitrate reduction; they also are produced in the diffusion-limited reaction of $NO^{\bullet}$ and superoxide, a reactive oxygen species (ROS). Thus, deoxygenation and RNS regulation are conceivable functions for TrHbs in these organisms.

Among RNS, $NO^{\bullet}$ is a focus of Hb research as these proteins are generally capable of $NO^{\bullet}$ dioxygenation.[13,15] The overall $NO^{\bullet}$ dioxygenase (NOD) reaction can be summarized as

$$\text{Hb–Fe(II)} + O_2 \leftrightarrows \text{Hb–Fe(III)}–O_2^- \quad (1)$$

$$\text{Hb–Fe(III)}–O_2^- + NO^{\bullet} \rightarrow [\text{Hb–Fe(III)}–OONO^-] \quad (2)$$

$$[\text{Hb–Fe(III)}–OONO^-] \rightarrow \text{Hb–Fe(III)} + NO_3^- \quad (3)$$

$$\text{Hb–Fe(III)} + e^- \rightarrow \text{Hb–Fe(II)} \quad (4)$$

To undergo multiple turnovers, the protein must be re-reduced to the O_2-binding competent ferrous state (step 4). Unlike the flavohemoglobins, which contain a flavin adenine dinucleotide (FAD) binding domain that allows for efficient heme redox cycling,[16] proteins such as THB1 would require intermolecular electron transfer to accomplish this last step.

$NO^{\bullet}$ plays a role as a signaling molecule in a variety of cellular processes, including several in the model organism *Chlamydomonas reinhardtii*, a close relative of *C. eugametos*. Specifically in the former, $NO^{\bullet}$ inhibits the import of ammonium, nitrite, and nitrate, and also nitrate reductase activity. These observations support the idea that $NO^{\bullet}$ can regulate the assimilation of nitrogen[17] and direct attention to the possible involvement of globins in processes related to $NO^{\bullet}$.

Several TrHb genes have been identified within the nuclear genome of *C. reinhardtii*. Following the current UniProtKB annotations, these are designated *THB1*–*THB4*, but at least 10 putative genes may contain TrHb domains.[8] Most *C. reinhardtii* TrHbs are hypothetical proteins. Exceptions are the products of "*THB8*", the level of expression of which is increased >1000-fold under anoxic conditions, and "*THB7*" and "*THB12*", which display mild upregulation under hypoxic conditions.[18] These proteins have not been characterized fully, and the chemistry associated with them is unclear. Recently, the gene product of *THB1* has been identified in *in vivo* work focused on intraflagellar transport (IFT) and the BBSome, an IFT cargo adaptor.[19] In this case, as well, functional information is missing.

Knowledge of amino acid sequences and *in vitro* properties far exceeds physiologic data for the TrHbs of cyanobacteria and unicellular photosynthetic algae.[20] In fact, it has been difficult to obtain biological information in part because these globins occur at relatively low levels and are generally not essential under most growth conditions. THB1 offers a rare opportunity to explore the properties of a TrHb and connect *in vitro* and *in vivo* information in a model organism. With the goals of testing specific functional hypotheses and relating *in vivo* and *in vitro* data, we report on the structure and reactivity of the purified recombinant protein and demonstrate the possible involvement of the protein in nitrogen metabolism.

MATERIALS AND METHODS

***Chlamydomonas* Cell Culture.** Strains CC-125, CC-1086, CC-1690, and CC-2453 were obtained through the Chlamydomonas Resource Center (University of Minnesota, St. Paul, MN). Strains g1 and *bbs4-1* were from the Witman lab. Cells were maintained on tris acetate phosphate (TAP) medium agar plates until the cells were used. Liquid cell cultures were grown in Sager-Granick M medium,[21,22] unless noted otherwise, at 20 °C under constant agitation and illuminated with cool white fluorescent light on a 14/10 (on/off) cycle to synchronize cell growth. For flagella isolation experiments, cells were aerated by being bubbled with 5% CO_2 and 95% air.

Antibody Production, Protein Analysis, and Gene Expression. Polyclonal antibodies were prepared using the synthetic peptide AADTAPADSLYSRC, which corresponds to the first 13 amino acids of THB1 (excluding the initial Met) followed by a single cysteine for covalent attachment to the keyhole limpet hemocyanin carrier protein. Antibodies were raised in rabbit (Covance, Princeton, NJ), affinity purified using the same synthetic peptide, and stored frozen at a protein concentration of approximately 1.5 mg/mL in phosphate-buffered saline (PBS) until they were used.

Whole cell protein was extracted from actively growing cultures of *C. reinhardtii* by resuspending approximately 1×10^7 cells/mL in 60 mM Tris-HCl (pH 7.0), 10% glycerol, 2% sodium dodecyl sulfate (SDS), and 50 mM tris(2-carboxyethyl)phosphine (TCEP, BondBreaker, Thermo Scientific), followed by boiling for 10 min and separating the protein on a 16.5% Tris-tricine SDS–polyacrylamide gel (Bio-Rad Laboratories, Hercules, CA). For silver staining, gels were fixed and stained according to manufacturer's protocol (Silver Stain Plus Kit, Bio-Rad). Flagellar isolation was performed using the dibucaine method as previously described.[23] In these experiments, whole cell samples were collected immediately prior to dibucaine treatment. After flagellar abscission, cell bodies were separated from flagella by centrifugation (3 min at 1150*g*). Concentrated whole flagella and corresponding whole cell and cell body proteins were separated on 4 to 15% Mini-PROTEAN TGX precast gels (Bio-Rad, Hercules, CA). For Western blots, the proteins were transferred to nitrocellulose (Whatman), blocked with dry milk, probed with appropriate antibodies, and detected using chemiluminescence. Rabbit polyclonal antisera (and dilutions) were anti-PLD (1:5000),[23] anti-BBS4 (1:2000),[19] and anti-βF_1-ATPase (1:80000).[24] Mouse monoclonal antibodies used were anti-IC2 (1:400)[25] and anti-IFT139 (1:20).[26]

For gene expression analysis, total cell RNA was extracted from actively growing cells using the RNeasy Plant RNA extraction kit with optional on-column DNA digest (Qiagen), and the quantity and purity of RNA were determined using a NanoDrop Spectrophotometer (Thermo Scientific). cDNA was synthesized from purified RNA using an iScript cDNA Synthesis kit (Bio-Rad) and analyzed using PrimeTime quantitative polymerase chain reaction (qPCR) probes (Table S1 of the Supporting Information) and 1× SsoFast Probes Supermix (Bio-Rad) on a Bio-Rad CFX Real Time Detection system using 40 cycles of 10 s, 95 °C melt steps and 20 s, 60 °C elongation steps per cycle. Normalized gene expression was calculated from biological duplicates performed in triplicate wells and normalized relative to the expression of the *CBLP* control gene[27] using CFX Manager.

dx.doi.org/10.1021/bi5005206 | *Biochemistry* 2014, 53, 4573–4589

Recombinant Protein Production. The coding sequence for the *THB1* gene was obtained from GenBank (EU095254.1) and used to create a synthetic gene that was inserted into the pJExpress414 plasmid after codon optimization for expression in a bacterial host system (DNA 2.0, Menlo Park, CA). Recombinant THB1 (below termed rTHB1) was obtained as described previously for *Synechocystis* sp. PCC 6803 GlbN.[28] As in this case, overexpression results in the production of the apoprotein, which fractionates into inclusion bodies. Following urea solubilization and gel filtration chromatography, the holoprotein was prepared by addition of excess hemin (Sigma) to refolded apoprotein, further purified by anion exchange chromatography, and lyophilized for storage at −20 °C as necessary.

Mass spectrometry was performed on an Acquity/Xevo-G2 UPLC-MS instrument (Waters) and returned a molecular mass of 14564 Da for purified rTHB1, in excellent agreement with the mass of 14564.4 Da expected for the polypeptide lacking the initial methionine. The protein concentration was determined on a per-heme basis with an extinction coefficient at 409 nm of 125 mM^{-1} cm^{-1} (ferric state, pH 7.0) obtained by the hemochromogen assay.[29,30] The apoprotein extinction coefficient was estimated to be 5.96 mM^{-1} cm^{-1} on the basis of the amino acid composition.[31]

Plasmids for Y29F and K53A rTHB1 production were obtained via QuikChange (Qiagen) mutagenesis of the pJexpress414 plasmid containing the codon-optimized *THB1* gene as per manufacturer's instructions. Primers were from Integrated DNA Technologies (Coralville, IA). Sequencing was performed by GENEWIZ, Inc. (South Plainfield, NJ). Overexpression and purification of the Y29F and K53A variants were performed in the same manner as for wild-type rTHB1.

O_2 Scavenging and Reduction Systems. When solutions needed to be scrubbed of dissolved O_2, the protein was incubated, and data were collected in the presence of the coupled glucose oxidase/catalase oxygen-scavenging system (GODCAT).[32] Final concentrations of the various components were 16.7 mM D-(+)-glucose (Amresco, Solon, OH), 0.02 mg/mL bovine catalase (Sigma), and 0.04 mg/mL *Aspergillus niger* glucose oxidase (Sigma).

When dithionite (DT) (Alfa Aesar, Ward Hill, MA) was not appropriate for reduction of the ferric protein, a ferredoxin (Fd)/$NADP^+$ reductase system[33] was used. Final concentrations of the various components (all from Sigma) were 0.04 mg/mL bovine catalase, 2.8−3.0 mM glucose 6-phosphate, 10 μM NADPH, catalytic amounts of *Leuconostoc mesenteroides* glucose-6-phosphate dehydrogenase, catalytic amounts of spinach Fd/$NADP^+$ reductase, and 30 μg/mL spinach Fd.

pH Titration of Ferric and Ferrous rTHB1 by Absorption Spectroscopy. The pH titration of ferric wild-type rTHB1 was obtained with a sample (15 μM) in 5 mM phosphate (pH 11.0). Spectra were obtained from 700 to 260 nm in ∼0.2 pH unit decrements achieved by adding 0.1 or 1 M HCl until a pH of 4.0 was reached. Complementary data were obtained from two separate titrations (acid range from pH 7.2 to 3.0 and base range from pH 7.2 to 13.0). The pH titration of ferric Y29F rTHB1 was obtained in a similar fashion in the pH ranges of 7.4−10.2, 7.4−3.3, and 9.0−14. A coarse pH titration of ferric K53A rTHB1 was performed between pH 4.8 and 10.2 in ∼1 pH unit increments. Data from ferric wild-type and Y29F rTHB1 between pH 5 and 10 over the 430 and 700 nm range were subjected to singular-value decomposition[34] using SciLab. Global fitting of significant vectors was performed with Savuka.[35]

The pH titration of ferrous wild-type rTHB1 was obtained from separate samples for each pH value from pH 4 to 10.8. Each sample contained ∼7 μM ferric rTHB1 in 100 mM buffer; different buffers were used depending on the desired pH (acetate/phosphate for pH 4.0−6.3, phosphate for pH 6.5−8, borax for pH 8.3−9.0, and glycine for pH 9.5−10.5). Spectra for each sample in the ferric state were collected prior to reduction to determine the concentration of the protein using the pH-dependent extinction coefficient determined in the ferric rTHB1 titration. Ferrous rTHB1 was then obtained by adding 2 mM DT to the sample, and the reduction was monitored as a function of time. Data points to form the titration curve were collected when the Soret band displayed maximal absorbance. The change in absorbance with time suggested damage to the protein caused by DT. The data may not correspond to a true equilibrium titration and are therefore less accurate than in the ferric state.

Ligand Binding Studies. Lyophilized ferric rTHB1 was dissolved in 100 mM phosphate buffer (pH 7.1) to generate a concentrated stock of the protein (∼2 mM). From this stock, samples containing ∼8 μM rTHB1 were prepared for the collection of absorbance spectra. The cyanomet complex (i.e., the ferric protein with cyanide bound as the distal ligand) was obtained by addition of a 5-fold excess of KCN. The ferric−$NO^•$ adduct [Fe(II)−NO^+] was prepared by addition of a 130-fold excess of $NO^•$ as released by 6-(2-hydroxy-1-methyl-2-nitrosohydrazino)-*N*-methyl-1-hexanamine (MAHMA-NONOate, Cayman Chemical, Ann Arbor, MI). In both cases, spectra were recorded until saturation was observed. The ferrous state was generated by incubation of the rTHB1 sample with GODCAT prior to the addition of DT. The ferrous cyano complex was obtained by reduction of the cyanomet complex with excess DT; likewise, the ferrous $NO^•$ adduct [Fe(II)−NO] was obtained by DT reduction of the ferric $NO^•$ adduct. O_2- and CO-bound rTHB1 samples were generated in buffer sparged with either O_2 (Air Gas, research grade, 99.999% pure) or CO gas (Air Gas, chemically pure grade, 99.5% pure) and reduced with either the Fd/$NADP^+$ reduction system or DT in the presence of GODCAT, respectively.

Nitric Oxide Dioxygenase and Griess Assays. The procedure used MAHMA-NONOate as the $NO^•$ donor and the Fd/$NADP^+$ reductase system for rTHB1 reduction. Specifically, ∼10 μM rTHB1 samples were prepared from a concentrated rTHB1 stock in 100 mM phosphate buffer (pH 7.1) equilibrated with air (∼21% O_2, 230 μM). The components of the Fd/$NADP^+$ reduction system were added except for Fd, and a reference UV−vis spectrum of ferric rTHB1 was collected. Approximately 30 μg of Fd was added (2.5 μM Fd, final concentration) to the sample, which resulted in observable Fd-mediated rTHB1 reduction. Absorbance data were collected from 600 to 300 nm every minute, with a scan rate of 600 nm/min.

Once rTHB1 was saturated with O_2, MAHMA-NONOate, quantitated by absorption spectroscopy at high pH (ε_{250} = 7.25 mM^{-1} cm^{-1}),[36] was added to the sample to generate 2 or 3 equiv of $NO^•$. The dead time for manual mixing was 15 s, after which the reaction of $NO^•$ with oxy rTHB1 was followed. Once the sample had recovered to the oxy state, a new addition of MAHMA-NONOate was made, and this protocol was repeated a total of five to eight times. As a control, a second sample containing buffer and the Fd/$NADP^+$ reductase system was

dx.doi.org/10.1021/bi5005206 | *Biochemistry* 2014, 53, 4573−4589

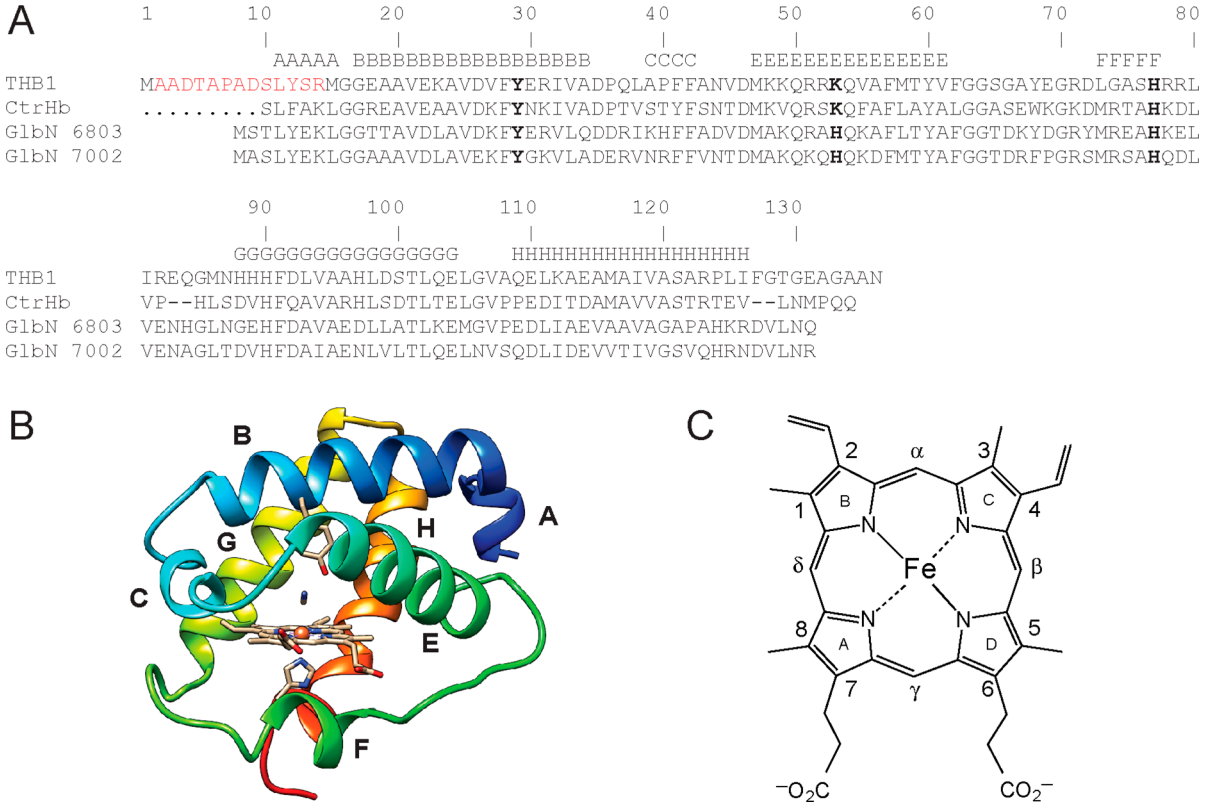

Figure 1. (A) Sequence alignment of THB1 and related TrHb1s: CtrHb, heme domain of *C. eugametos* LI637; GlbN 6803, GlbN from *Synechocystis* sp. PCC 6803; GlbN 7002, GlbN from *Synechococcus* sp. PCC 7002. The sequence numbering is for THB1. Helices are denoted A–H according to the secondary structure of CtrHb (PDB entry 1DLY) and Perutz notation. Residues of interest are His77 (the proximal histidine, His F8), Tyr29 (termed "B10" by analogy to the three-dimensional structure of mammalian Hbs), and Lys53 ("E10"). These positions are highlighted in bold. The N-terminal sequence is colored red and was used to raise anti-THB1 antibodies. (B) Structural model of THB1 prepared with SWISS-MODEL.[49] The program selected CtrHb with bound cyanide (PDB entry 1DLY) as the best template for homology modeling.[49] (C) *b* Heme structure and numbering.

prepared with no rTHB1 present ("−THB1") and was treated in the same manner as the sample containing rTHB1 ("+THB1"). Horse skeletal muscle Mb (Sigma) was subjected to an analogous procedure for the purpose of comparison. The kinetics of MAHMA-NONOate decomposition were determined in an independent experiment and yielded a half-life of 2–3 min at pH 7 (not shown).

Nitrite was quantitated at the end of each experiment using the Griess assay.[37] The NOD reaction mixtures were split into two fractions to which 4 μM FAD (final concentration) was added. To one of these samples was added *A. niger* nitrate reductase (NR, Sigma) to a final concentration of 0.075 unit/mL along with an NADPH regeneration system[38] to convert nitrate into nitrite stoichiometrically. After ~20 min, both samples were treated with the Griess reagents (GR) as per the manufacturer's instructions (Life Technologies, Grand Island, NY). Absorbance spectra were collected from 600 to 300 nm every minute until complete conversion was reached by the sample containing the largest amount of nitrite (20–50 min). Nitrite concentrations were obtained from a calibration curve produced under the same conditions that were used for the NOD reaction and yielded an ε_{520} of 26.9 μM^{-1} cm^{-1} for the diazonium product. The same protocol was used to determine the amount of nitrate produced in NOD reactions in the presence of horse skeletal muscle Mb. Kinetic simulations were performed with KinTek Explorer.[39]

UV–Visible Spectrophotometry. Absorbance spectra were collected on either a Varian Cary-50 or an AVIV 14DS instrument. For extinction coefficient measurement, pyridine hemochrome spectra were acquired in triplicate, from 600 to 500 nm in 1 nm steps, using a 1 s averaging time per step. Ligand binding, NOD, and Griess assays were monitored using the Cary50 scanning kinetics mode. Optical spectra were collected using an averaging time of 0.1 s, from 700 to 300 nm, every 60 s, until sample equilibration was achieved.

NMR Spectroscopy. NMR data were acquired at 14.1 T with a Bruker Avance or Avance II spectrometer equipped with a cryoprobe. ^{1}H chemical shifts were referenced to 2,2-dimethylsilapentane-5-sulfonic acid through the temperature-corrected $^{1}H_2O$ line (4.76 ppm at 298 K). ^{13}C and ^{15}N chemical shifts were referenced indirectly in accordance with their respective Ξ ratios.[40] NMR data were processed using NMR Pipe 3.0[41] or TopSpin 2.1 (Bruker BioSpin, Rheinstetten, Germany). Analysis of NMR spectra was completed using Sparky 3.[42]

Unlabeled or uniformly ^{15}N-labeled rTHB1 samples were exchanged from 50 mM Tris purification buffer into 300 μM phosphate or 20 mM phosphate (pH 7.5–8.0, 10% $^{2}H_2O$) and first examined in the ferric state in the absence of an exogenous ligand. Ferric wild-type, Y29F, and K53A rTHB1 samples ranged from 500 μM to 3 mM heme in 270–600 μL at pH 7.0–7.6. Initial ^{1}H spectra were collected at either 298 or 308 K over a large spectral width to detect high-spin species. An

dx.doi.org/10.1021/bi5005206 | *Biochemistry* 2014, 53, 4573–4589

increased population of the high-spin form of ferric rTHB1 was achieved by lowering the sample pH to 5.4 at 298 K.

To generate the ferrous state of wild-type, Y29F, and K53A rTHB1, a ~2 mM protein solution [25 mM borate (pH 9.1–9.5)] was placed in a glovebox under a continuous Ar (AirGas purity 4.8) stream. After approximately 10 min, the protein was reduced with 2.5 molar equiv of DT. The solution was transferred to an NMR Shigemi tube, and the tube was sealed with Parafilm. Samples produced in this manner remained completely reduced over the time scale of NMR data acquisition (days to weeks). Ferrous ^{15}N-labeled WT and unlabeled Y29F and K53A rTHB1s were investigated by collecting one-dimensional (1D) ^{1}H spectra with water presaturation. ^{1}H–^{15}N HSQC, ^{1}H–^{15}N histidine selective long-range HMQC data were collected on the wild-type protein, and homonuclear two-dimensional (2D) NOESY and DQF-COSY data were acquired on the Y29F variant as described previously.[43]

For electron self-exchange (ESE) measurements, a 1.8 mM sample of ferric wild-type [^{15}N]rTHB1 in 250 mM borate (pH 9.2) and a 10% $^{2}H_2O$/90% $^{1}H_2O$ mixture was incubated with GODCAT and purged with Ar as described above. A substoichiometric amount of DT was added, resulting in a mixture containing ferric and ferrous protein in an ~2.2:1 ratio. As estimated by the relative integrated intensities of resolved amide signals in relaxed ^{1}H–^{15}N HSQC spectra, the ferrous and ferric populations remained stable over the course of 24 h (final ferric:ferrous ratio of ~2.6:1).

The kinetics of ESE were estimated on a mixture of ferric and ferrous rTHB1 using a ^{1}H–(N_Z)–^{1}H ZZ exchange experiment. The sample was initially screened by comparing standard ^{15}N–^{1}H HSQC data with a ^{15}N–(N_Z)–^{1}H 2D ZZ exchange spectrum (ZZ mixing time of 452 ms) recorded as detailed previously.[44] The small difference in ^{15}N shifts between ferrous and ferric forms necessitated the use of ^{1}H–(N_Z)–^{1}H 2D ZZ exchange data.[44,45] N_Z ZZ mixing times were 452, 271, 701, 158, 565, 362, 1018, and 452 ms. $^{1}H_Z$–$^{15}N_Z$ heteronuclear cross-relaxation was minimized with 1.3 ms G3 ^{1}H inversion pulses every 10 ms during the N_Z mixing time; these pulses were applied 2800 Hz downfield of the $^{1}H_2O$ line to limit the saturation of water magnetization, which was maintained at equilibrium during the ZZ period. Because of the low cross-peak intensity and sample variation with time, the data provide an estimate of the lower limit of the kinetics of ESE.

The cyanomet state of rTHB1 was prepared by incubation of ferric rTHB1 with a 1.5–6-fold molar excess of potassium cyanide for at least 30 min prior to data acquisition. Cyanomet wild-type rTHB1 samples were prepared at pH 7.5; protein concentrations ranged from 2 to 5.5 mM in either 10% or 99.9% $^{2}H_2O$ solutions. Data were acquired at 298 K. ^{1}H homonuclear data (1D, NOESY, and DQF-COSY) and natural abundance ^{1}H–^{13}C HMQC data were collected on both wild-type and Y29F rTHB1 under similar conditions. In addition, wild-type rTHB1 was studied using ^{1}H–^{1}H TOCSY, ^{1}H–^{15}N HSQC, ^{1}H–^{15}N histidine selective long-range HMQC, three-dimensional (3D) NOESY-HSQC, and 3D TOCSY-HSQC experiments as described previously.[46−48]

RESULTS AND DISCUSSION

Figure 1A presents the primary structure of THB1, which has the features of a "group I" TrHb (TrHb1 for short), one of three branches of the TrHb family.[2] Of the few TrHb1s that have been studied, the closest relatives are also shown: *C. eugametos* LI637[4] (CtrHb, 48% identity) and the cyanobacterial globins from *Synechocystis* sp. PCC 6803 (49% identity) and *Synechococcus* sp. PCC 7002 (46% identity). The three-dimensional structures of these proteins are available in the cyanomet form [Protein Data Bank (PDB) entries 1DLY, 1S69, and 4L2M, respectively]. The Cα traces of the three structures superimpose with root-mean-square deviations of <0.8 Å over 90% of the chain. This similarity raises the expectation that the TrHb1 fold is robust and representative of THB1. The structure of cyanomet CtrHb with appropriate amino acid replacements (Figure 1B, prepared with SWISS-MODEL)[49] was used to guide the analysis of the rTHB1 NMR data.

Purified rTHB1 appeared as a single band on silver-stained SDS–polyacrylamide gels (Figure 2A, lane 1). The heme-

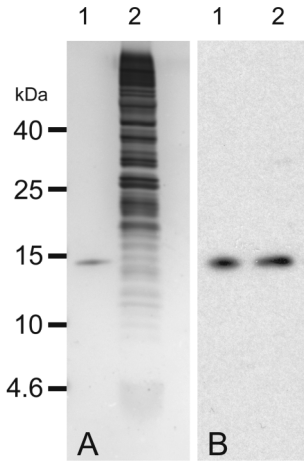

Figure 2. Comparison of rTHB1 and *in vivo* THB1: (A) 1 μg of rTHB1 (lane 1) and 1 × 10^5 cells of CC-1690 grown in Sager-Granick M medium (lane 2) analyzed via SDS–polyacrylamide gel electrophoresis (PAGE) and stained with silver and (B) 0.5 ng of rTHB1 (lane 1) and 1 × 10^5 cells of CC-1690 grown in Sager-Granick M medium (lane 2) separated via SDS–PAGE and transferred to nitrocellulose followed by immunodetection using purified polyclonal rabbit antibodies raised against a THB1 peptide.

reconstituted protein is highly soluble in aqueous buffer and has a far-UV circular dichroism spectrum consistent with the helical content of CtrHb (Figure S1 of the Supporting Information). The high affinity of rTHB1 for heme and its reproducible behavior in solution suggest that this protein can serve as a good substitute for endogenous THB1. The characterization of the purified protein was initiated with optical spectroscopy to gain insight into heme coordination, association with various diatomic ligands, and stability to acid.

rTHB1 Binds Diatomic Ligands. Figure 3A–D shows the absorption spectra of rTHB1 with and without the usual complement of diatomic ligands at neutral pH: O_2, CO, and $NO^{\bullet}$ in the ferrous state and CN^- and $NO^{\bullet}$ in the ferric state. Of note is the formation of the cyanide adduct of the ferrous state (Figure 3C) by DT reduction of cyanomet rTHB1. Ferrous cyano rTHB1, however, could not be obtained by addition of cyanide to reduced rTHB1. Absorbance maxima and extinction coefficients are listed in Table 1. Each spectrum is distinctive and can be used for the purpose of identifying species occurring in mixtures and enzymatic assays.

pH Dependence of Heme Axial Coordination in Ferric rTHB1. Figure 4 and Figure S2 of the Supporting Information illustrate the pH response of rTHB1 monitored via absorbance

dx.doi.org/10.1021/bi5005206 | *Biochemistry* 2014, 53, 4573–4589

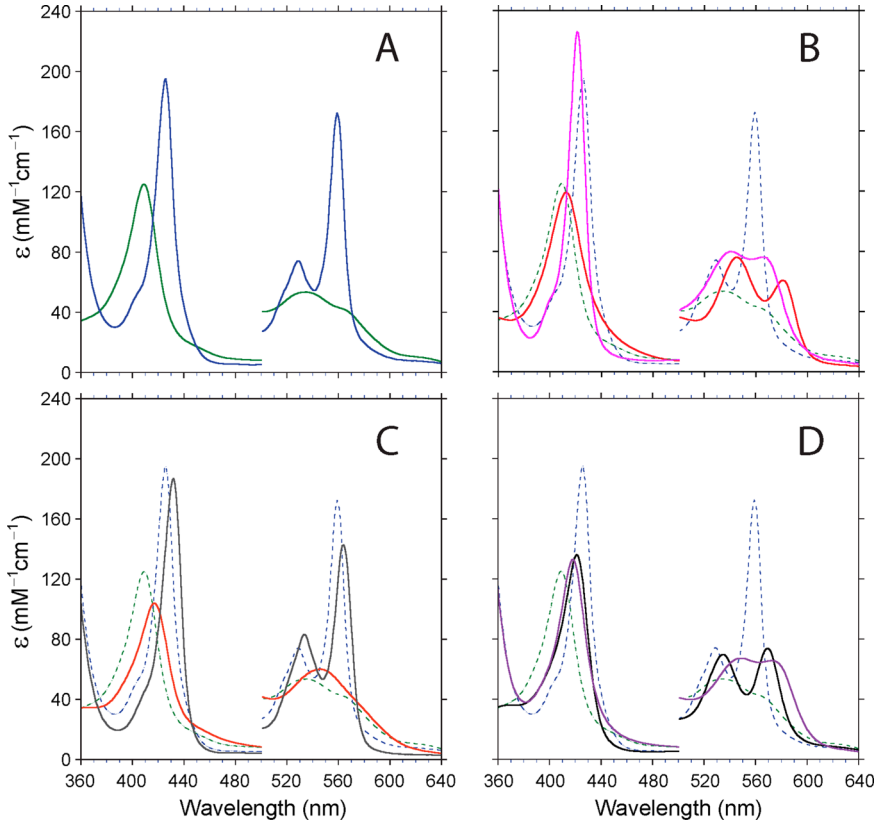

Figure 3. Absorption spectra of various forms of rTHB1 (~10 μM, 100 mM phosphate buffer, pH 7.1). The vertical scale was adjusted to provide the extinction coefficient, ε in mM^{-1} cm^{-1}. The intensity of the α–β band region was magnified by a factor of 5. (A) Ferric (green) and ferrous (blue) proteins at pH 7.1. These two spectra are reproduced with dashed lines in panels B–D. (B) Oxy (red) and carbonmonoxy (magenta) states. (C) Cyanide complexes of the ferrous (gray) and ferric (orange) states. (D) $NO^{\bullet}$ adducts of the ferrous (purple) and ferric (black) states.

Table 1. Optical Properties of Various Wild-Type rTHB1 Complexes at pH 7.1

protein state	Soret maximum (nm)	α (nm)	β (nm)	CT[a] (nm)	ε at Soret maximum (mM^{-1} cm^{-1})
Fe(III) (pH 4.8)	408	503, 542 (sh)		630	144
Fe(III) (pH 7.1)	410	536, 568 (sh)		630 (sh)	125
Fe(III) (pH 10.8)	412	538, 570 (sh)			118
Fe(II)	426	529	559		195
Fe(III)–CN^-	417	546			104
Fe(II)–CN^-	432	534	564		187
Fe(III)–NO	421	535	570		136
Fe(II)–NO	418	548	573		133
Fe(II)–O_2	412	545	581		119
Fe(II)–CO	421	541	564		226

[a]Charge transfer band.

measurements in the absence of added ligand. Below pH 4.8, the Soret band experiences a sharp decrease in intensity (apparent pK_a of 3.72 ± 0.01 and a Hill coefficient of 3.45 ± 0.15, where the uncertainties are the errors of the fit); a shallower drop occurs at pH >10.8 (apparent pK_a of 12.49 ± 0.01 and a Hill coefficient of 1.25 ± 0.03). Both acid and alkaline transitions (Figure S2 of the Supporting Information) are accompanied by spectral alterations between 400 and 700 nm characteristic of a change in heme coordination. The acid transition is likely coupled with protonation of the proximal histidine, the loss of heme from the protein cavity, and protein unfolding, whereas the nature of the alkaline transition is unclear as the spectral features at very high pH (broad absorption band at 588 nm, Soret maximum at 398 nm, and shoulder at 350 nm) do not match those of free hemin under the same conditions.

The spectral response in the range of pH 4.8–10.8 is shown for the visible region in Figure 4A. Figure 4B presents the pH titration curve described by the absorbance at 540 nm. The 430–700 nm data, when analyzed by singular-value decomposition,[34] yield two principal abstract vectors. Global fitting[35] returns an apparent pK_a of 6.48 ± 0.07 with a Hill coefficient of 0.86 ± 0.03 and indicates a transition involving one proton. However, imperfect isosbestic points (482, 522, and 598 nm) and the sloping baselines required to achieve a good fit (Figure 4B) hint at the participation of an additional low-population species or secondary ionization event.

The main spectral component between pH 4.8 and 6.5 is consistent with a high-spin, water-bound species.[50] In contrast, the main component between pH 6.5 and 10.8 has low-spin character and is not readily recognized. Its appearance eliminates the possibility of a ferric hydroxy complex[50] or a ferric pentacoordinate species[51] and supports coordination of a protein residue to the iron on the distal side. This behavior parallels that of ferric CtrHb.[52]

pH Dependence of Heme Axial Coordination in Ferrous rTHB1. The response of ferrous rTHB1 to pH, shown in Figure 4C, is also reminiscent of that observed for CtrHb. Between pH 7 and 10, the protein spectrum is consistent with that of a six-coordinate low-spin complex.[53] At

dx.doi.org/10.1021/bi5005206 | Biochemistry 2014, 53, 4573–4589

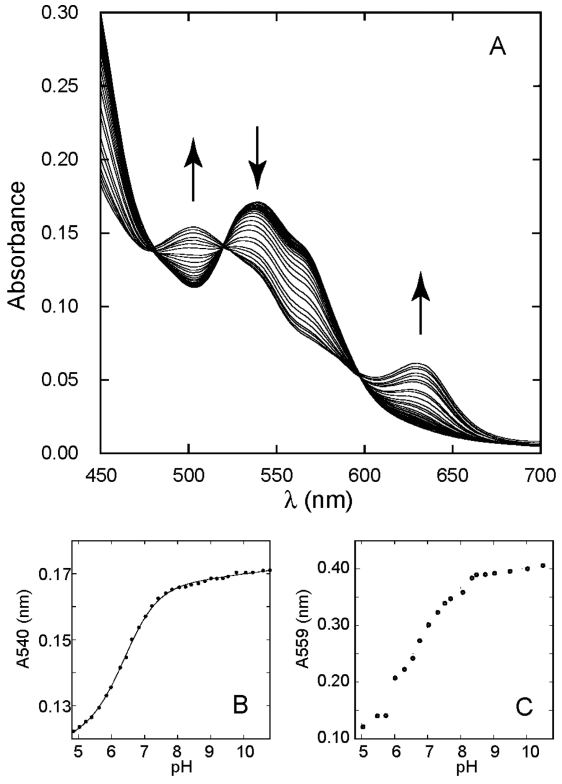

Figure 4. pH titration of rTHB1. (A) The α and β bands of the ferric protein are shown between pH 10.8 and 4.8. The vertical arrows indicate the direction of the change as the pH is decreased. (B) Absorbance of the ferric protein at 540 nm as a function of pH. The solid line is the result of fitting the data according to a modified Henderson–Hasselbalch equation assuming a single ionization event [pK_a = 6.48 (see the text)]. (C) Absorbance of the ferrous protein at 559 nm as a function of pH.

acidic pH, the spectral features of a four-coordinate heme[53] emerge with broad Soret and α–β bands suggesting loose association of the heme with the protein. The intermediate state, presumably a five-coordinate species with the proximal histidine as sole axial ligand, does not become highly populated under the explored conditions, although there is evidence of this state at neutral pH (Figure S3 of the Supporting Information). The apparent pK_a for the global six-coordinate to four-coordinate transition is ~6.6.

Optical Data for the Endogenous Coordination on the Distal Side. Two plausible candidates for axial coordination on the distal side of the heme are the residues at position B10, as proposed in CtrHb,[52] and E10, as in the two cyanobacterial GlbNs introduced in Figure 1A.[54,55] In THB1, Tyr29 occupies the B10 position and Lys53 the E10 position. To determine the identity of the distal ligand, we first replaced Tyr29 (B10) with a phenylalanine. The Y29F variant binds heme tightly and yields optical spectra (not shown) similar to those of the wild-type protein. In addition, the pH response has transitions in the acidic, neutral, and alkaline regions that match closely those of the wild-type protein (Figure S2 of the Supporting Information). In particular, the transition near neutral pH occurs with an apparent pK_a of 6.82 ± 0.05 and a Hill coefficient of 0.97 ± 0.05, obtained by global fitting. The minor perturbations caused by the Y29F replacement suggest that, in ferric wild-type THB1, Tyr B10 is not an axial ligand to the iron.

In contrast, the K53A replacement causes pronounced changes in the optical spectrum and its pH response. At neutral pH, ferric K53A rTHB1 has a spectrum (Figure 5)

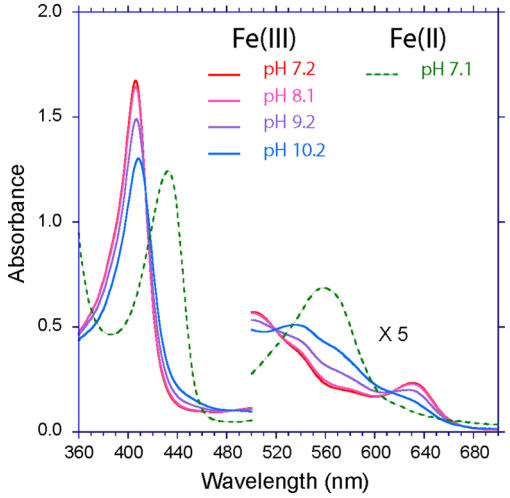

Figure 5. Optical spectrum of K53A rTHB1 in the ferric state at four pH values and in the reduced state at pH 7.1. The ferric state undergoes an aquomet–hydroxymet transition at pH >8.

reminiscent of ferric wild-type and Y29F rTHB1 at acidic pH, indicating the presence of a water molecule on the distal side of the heme and the absence of a sixth endogenous ligand. There is little change in the spectrum from pH 5 to 8 (Figure S4 of the Supporting Information). Starting at pH ~8, the Soret band, the Q-band, and charge transfer band begin to decrease as the pH is increased. At pH 10, the charge transfer band has almost disappeared and both the Soret band and the Q-band shift to the red (Soret maximum of 406–408 nm; Q range of 502–534 nm) in an apparent aquomet–hydroxymet transition. These data implicate Lys53 (E10) as the distal ligand to the iron responsible for the six-coordinate low-spin features detected optically in wild-type and Y29F rTHB1. The absence of a 602 nm maximum in these spectra also suggests that Tyr B10 does not coordinate the iron when K53 is removed.[56] Interestingly, the spectra of ferric and ferrous wild-type and Y29F rTHB1 resemble those reported for the Met100Lys variant of cytochrome c_{550},[57] with allowance for a blue shift caused by the thioether cross-links in the cytochrome. Similarity to complexes with N–Fe–N coordination is also noted.[58]

NMR Data for the Identification of Lys53 as the Distal Axial Ligand. Optical spectra have limited information content, and amino acid replacements can have unanticipated consequences; confirmation of the ligation scheme was therefore pursued by NMR spectroscopy. At pH 7.6, the ^{1}H spectrum of ferric rTHB1, shown in Figure 6A, contains moderately shifted resonances supporting a predominant low-spin complex. The spectrum also showed a minor population of low-intensity, far-downfield broad resonances characteristic of a high-spin ($S = {}^5/_2$) complex.[59] In accordance with the absorbance data, the population of this high-spin form increased when the pH was decreased (Figure 6B) and was therefore attributed to an aquomet species. As the pH was increased above 8, the broad lines disappeared, and only the spectrum with comparatively narrow features could be detected (not shown). At pH 7.0, the Y29F variant also displays a

dx.doi.org/10.1021/bi5005206 | Biochemistry 2014, 53, 4573–4589

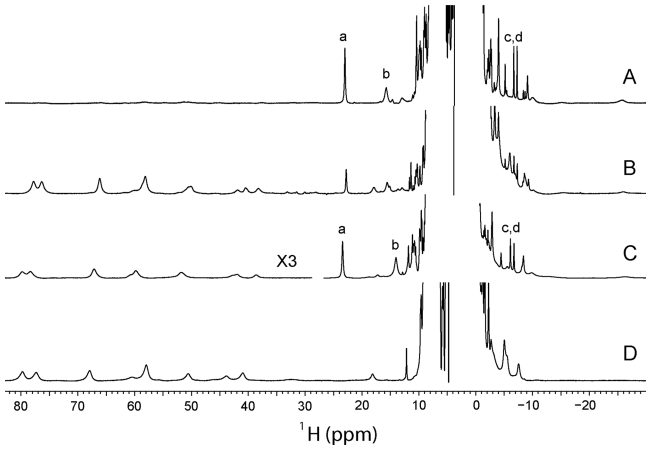

Figure 6. One-dimensional ^{1}H spectra of ferric rTHB1: (A) wild type at pH 7.6 (~9% high-spin), (B) wild type at pH 5.4 (intensity ×4 compared to trace A, ~90% high-spin), (C) Y29F variant at pH 7.0 (intensity of downfield region ×3, ~40% high-spin), and (D) K53A variant at pH 7.4. Resonances marked a–d correspond to the 3-CH_3, 8-CH_3, and 2-vinyl β_{trans} and β_{cis} protons, respectively, from the low-spin wild-type and Y29F species. Data were recorded in a 10% ^2H_2O/90% ^1H_2O mixture at 298 K.

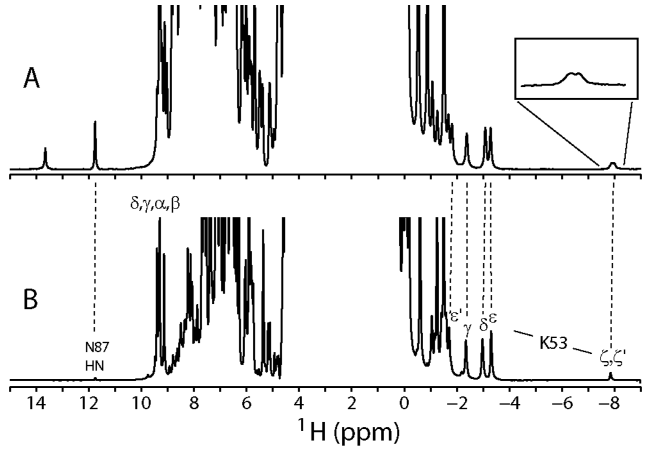

Figure 7. ^{1}H spectra of ferrous rTHB1. One-dimensional spectra of (A) ^{15}N-labeled wild-type rTHB1 in a 90% ^1H_2O/10% ^2H_2O mixture (pH 9.5) with amide ^{15}N decoupling (120 ppm) during acquisition and (B) Y29F rTHB1 in a 10% ^1H_2O/90% ^2H_2O mixture (pH* 9.2). Heme meso, Asn87 NH, and resolved Lys53 signals are labeled.

predominant low-spin species (Figure 6C). In contrast, the K53A rTHB1 spectrum at neutral pH contains only the resonances of an aquomet complex (Figure 6D). As the pH is increased to 9.1, a broad spectrum consistent with mixtures of aquomet and hydroxymet forms is obtained (not shown).

Analysis of ^{1}H–^{13}C HMQC and DQF-COSY data identified the ring signals from Tyr29 and Phe29 in wild-type and Y29F rTHB1, respectively (Figure S5 of the Supporting Information). The moderate line widths and modest downfield shifts of Tyr29 ring protons are inconsistent with ligation to the heme iron. In neither case were any NOE contacts observed between the aromatic ring at position 29 and the heme cofactor. Signals from a potential sixth ligand were not immediately apparent in these spectra.

In the proximity of the iron, paramagnetic effects can broaden lines and render resonance identification difficult. These effects were attenuated by reduction to the ferrous state, which was conducted at high pH (9–9.5) to populate fully the diamagnetic complex according to the optical data. The water presaturation ^{1}H 1D spectrum of ferrous wild-type rTHB1 (Figure 7A) and ferrous Y29F rTHB1 (Figure 7B) at pH 9.5 (10% ^2H_2O/90% ^1H_2O) and pH* 9.2 (90% ^2H_2O/90% ^1H_2O), respectively, revealed a set of six single-proton resonances between −1.4 and −3.4 ppm. Such large upfield shifts are expected of nuclei directly above and below the porphyrin macrocycle. These signals are absent from the spectra of the K53A variant (Figure S6C of the Supporting Information). In agreement with expectations, of the reduced proteins only K53A rTHB1 shows broad features typical of $S > {}^1/_2$ states (Figure S6C–E of the Supporting Information).

J correlation data [DQF-COSY (Figure 8A)] collected on Y29F rTHB1 unequivocally connect the upfield-shifted signals and trace a -CH-$(CH_2)_4$- system attributed to a lysine. NOE data (Figure 8B–D) confirmed dipolar contact with three of the four heme meso protons. Assignments are provided in Table S2 of the Supporting Information. A strikingly similar set of aliphatic resonances has been reported for the Met100Lys variant of cytochrome *c*[57] and lends further support to the ligation of a lysine to the iron. In addition, a resonance corresponding to two labile protons was detected at −7.8 ppm. Strong NOEs to the lysine aliphatic chain (Figure 8B) and to the heme α meso proton (not shown) and splitting into a doublet in ^{15}N-labeled samples (Figure 7A) secure assignment to the NζH_2 of the lysine. The chemical shifts of the Lys53 side chain are listed in Table S3 of the Supporting Information. We conclude that the distal ligand in ferrous rTHB1 is Lys53. To the best of our knowledge, this is the first documented example of a His–Fe–Lys coordination scheme in a hemoglobin.

The pH titrations of ferric and ferrous wild-type rTHB1 (Figure 4) suggest that K53 is a heme ligand in the ferric state. To test this hypothesis, we sought to measure ESE in wild-type rTHB1. A sample of uniformly ^{15}N-labeled ferric wild-type rTHB1 was prepared at pH 9.2 to favor the endogenous hexacoordinate state (Figure 4). Substoichiometric addition of DT resulted in a mixture of ferrous and ferric rTHB1. In fully relaxed ^{1}H–^{15}N HSQC spectra, the downfield-shifted amide NH signals from Asn87 (see below) report on the proportion of reduced and oxidized species. The mixture shown in Figure 9 originally contained approximately 31% reduced rTHB1. Little oxidation occurred during the course of data acquisition (28% reduced rTHB1 present at the end). Two-dimensional ^{1}H–(N_Z)–^{1}H data were collected to take advantage of the resolved ^{1}H shifts and the apparent slow exchange between the two states. The observation of specific cross peaks connecting corresponding ferrous and ferric amide NH resonances is direct evidence that under these conditions, an electron transfer event interconverts the redox forms of rTHB1.

In favorable cases, measurement of the cross and diagonal peak intensities as a function of the N_Z mixing time provides data for determining the rate constant of exchange.[60] The population drift and low signal-to-noise ratio prevented a detailed analysis of the exchange process, but an estimate could be obtained from the backbone amide cross peak of Asn87. An effective ESE rate constant was found to be 0.4 s^{-1} at 1.8 mM total protein (apparent second-order rate constant of ~0.2 mM^{-1} s^{-1}). Although this number pertains to nonphysiological conditions, it indicates that rTHB1 can exchange electrons at a rate ~1 order of magnitude slower than that of the bis-histidine GlbNs under similar conditions.[44] ESE kinetics have been measured from 10^7 to 10^2 M^{-1} s^{-1} in a variety of heme proteins,

dx.doi.org/10.1021/bi5005206 | *Biochemistry* 2014, 53, 4573–4589

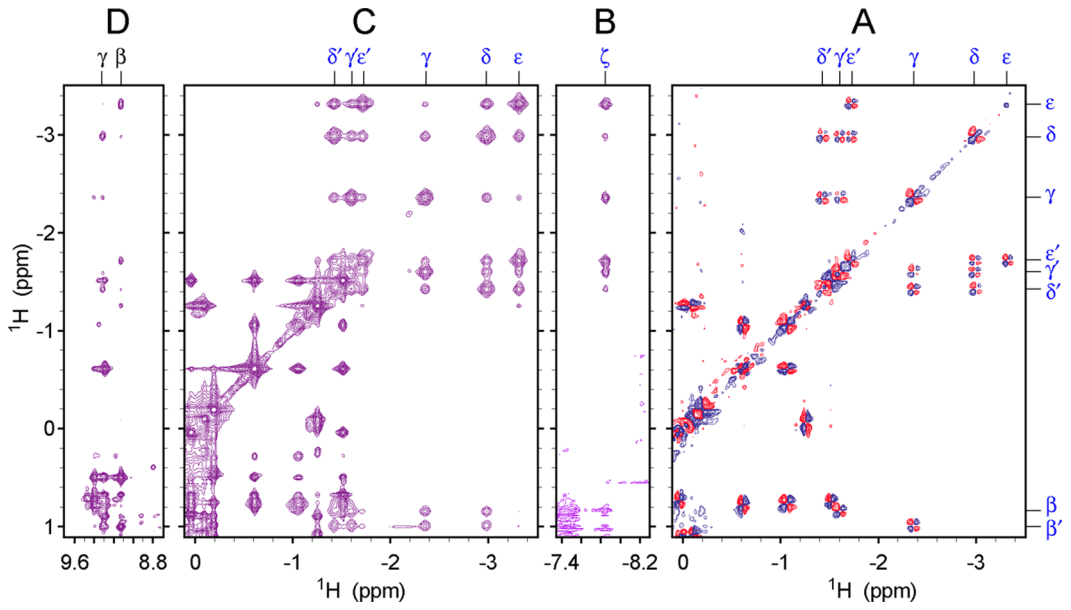

Figure 8. Two-dimensional ^{1}H data collected on ferrous Y29F rTHB1. (A) Upfield portion of the DQF-COSY data. (B–D) Regions of the NOESY data mapping the Lys53 spin system and indicating contact with the heme β and γ meso protons. Data were recorded in a 10% ^1H_2O/90% ^2H_2O mixture at 298 K and pH* 9.2. Blue symbols in panels A–C denote Lys53 signals. Black symbols in panel D denote heme meso signals.

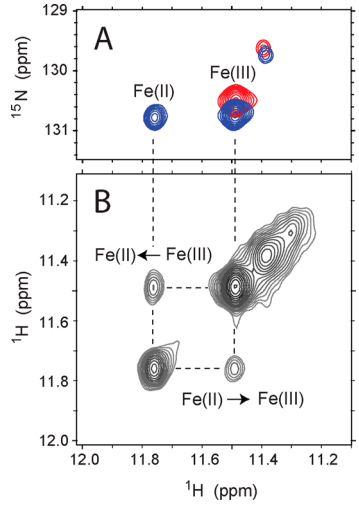

Figure 9. ESE in wild-type rTHB1. (A) Portion of a ^{1}H–^{15}N HSQC spectrum collected on a 3:7 mixture of ferrous and ferric rTHB1 (blue, 1.8 mM rTHB1, pH 9.2, 298 K) superimposed over that of a sample of pure ferric rTHB1 (red, pH 7.5, 298 K). The cross peaks are from Asn87 NH. (B) Matching region of a ^{1}H–($^{15}N_Z$)–^{1}H ZZ exchange NMR spectrum (τ_{mix} = 701 ms) recorded on the ferrous/ferric mixture. The square pattern is caused by redox interconversion.

including cytochromes *c* (His-Met, 10^7–10^2 M^{-1} s^{-1}), cytochromes b_5 (His-His, 10^5–10^4 M^{-1} s^{-1}), and aforementioned GlbNs (His-His, 10^3–10^2 M^{-1} s^{-1}).[61] The rather slow kinetics for rTHB1 suggest that structural reorganization may limit the rate of electron transfer. Rapid lysine decoordination or solvent exchange dynamics may explain the slow but detectable ESE and be responsible for the broad line shape of the Lys53 NζH_2. Overall, the data are consistent with Lys53 being the reversible distal ligand in both the ferric and ferrous states of rTHB1.

Cyanomet rTHB1 Has a Distal H-Bond Network. Upon addition of cyanide, the ^{1}H NMR resonances of rTHB1 sharpen significantly (Figure 10A). This complex is stable and was chosen for the study of a representative species with a bound exogenous ligand. The number and intensity of hyperfine-shifted resonances indicate that two forms of the protein coexist in a 5.5:1 ratio. Heme signals from both forms are readily assigned with homonuclear NOESY, DQF-COSY, and TOCSY data, aided by natural abundance ^{1}H–^{13}C HMQC spectra. Resonance attribution is performed on the basis of ^{13}C shift, ^{1}H intensity, and ^{1}H–^{1}H scalar coupling patterns (Figure S7 of the Supporting Information contains the vinyl couplings). Assignment to specific peripheral substituents (Figure 1C) is achieved using intra-heme NOE connectivities. For example, the 1-CH_3/2-vinyl and 3-CH_3/4-vinyl pairs are distinguished by the observation of a small 8-CH_3-to-1-CH_3 effect. Figure S8 of the Supporting Information shows the heme group with relevant intra-heme NOEs. Table 2 lists the chemical shifts of the heme peripheral substituents. The heme methyl chemical shift pattern displayed by the minor form is consistent with heme orientational isomerism,[59] as are NOEs (not shown).

The conformation of the distal pocket, where exogenous ligands bind and chemistry usually occurs, is an important determinant of reactivity. In cyanomet rTHB1, two exchangeable protons, not split into a doublet when the protein is uniformly labeled with ^{15}N, are detected at 27.0 ppm (major isomer) and 24.8 ppm (minor isomer) (Figure 10A). These efficiently relaxed protons have strong NOEs to resonances at 10.2 ppm (major isomer) and 9.68 ppm (minor isomer), themselves *J*-coupled to signals at 8.12 and 7.90 ppm, respectively. ^{13}C data (Figure S9 of the Supporting Information) prescribe assignment to Hδ and Hε resonances of two (major and minor) tyrosine rings rotating rapidly about their Cγ–Cζ axis. Similar sets of OηH and ring signals are detected in other cyanomet TrHb1 spectra[62,63] and are characteristic of Tyr B10 as it forms a hydrogen bond to the axial cyanide. In rTHB1, this residue is Tyr29, as confirmed with partial sequential assignments secured with ^{15}N-separated NOESY and TOCSY data. Ring-to-ring NOEs to the adjacent Phe28 indicate a geometry compatible with that of CtrHb (PDB entry 1DLY). Consistent with this, the spectrum of

dx.doi.org/10.1021/bi5005206 | *Biochemistry* 2014, 53, 4573–4589

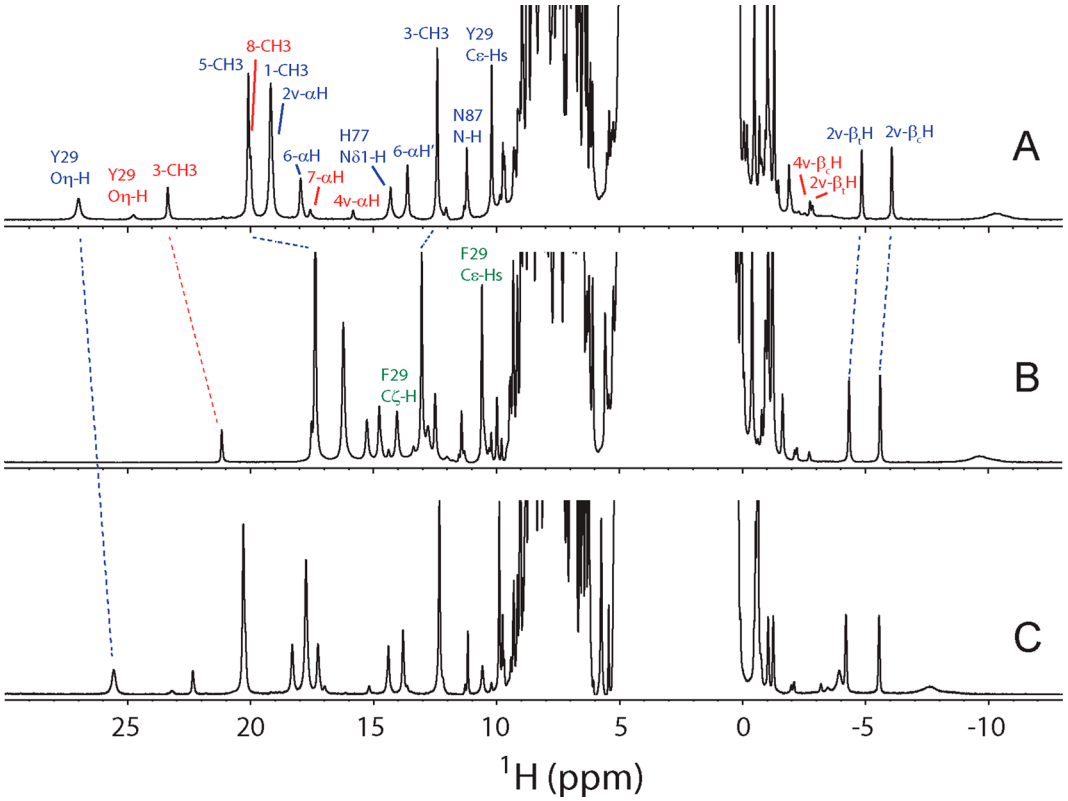

Figure 10. One-dimensional ^{1}H spectra of cyanomet rTHB1s at 298 K in a 10% ^2H_2O/90% ^1H_2O mixture: (A) wild type at pH 7.5, (B) Y29F variant at pH 7.4, and (C) K53A variant at pH 7.7. Select assignments are indicated on panels A and B as listed in Table 2 and Tables S4–S6 of the Supporting Information. Blue labels refer to the major heme orientational isomer, red labels to the minor isomer, and green labels to Phe29 within the Y29F variant.

Table 2. ^{1}H and ^{13}C Chemical Shifts of the Heme Group in Cyanomet Wild-Type rTHB1[a]

	major isomer		minor isomer	
assignment	^{1}H	^{13}C	^{1}H	^{13}C
1-CH_3	19.09	−32.1	2.62	−7.8
2-α-vinyl	19.06	36.6	9.78	72.6
2-β-vinyl *cis, trans*	−6.00, −4.76	204.6	−1.93, −2.83	
3-CH_3	12.27	−29.1	23.24	−39.6
4-α-vinyl	4.89	61.6	15.78	61.7
4-β-vinyl *cis, trans*	−0.68, 0.27	135.6	−2.72, −1.42	176.9
5-CH_3	20.3	−36.9	5.54	−14.2
6-α-propionate	18.09, 13.60	−39.5	5.95, 3.88	
6-β-propionate	0.92, 0.03		−0.75, −1.38	
7-α-propionate	4.89, 3.43		17.67, 12.05	−33.2
7-β-propionate	−1.10, −1.82	77.7	1.36, 0.65	
8-CH_3	5.00	−14.4	20.23	−35.2

[a] δ (parts per million), determined in 99.9% ^2H_2O at pH* 7.5, 300 μM phosphate, and 25 °C on a 5.5 mM wild-type rTHB1 sample with a 2-fold excess of KCN.

cyanomet Y29F rTHB1 (Figure 10B) does not contain any labile proton resonances downfield of 16 ppm, whereas the cyanomet K53A rTHB1 variant displays a ^{1}H NMR spectrum (Figure 10C) similar to that of the wild-type protein and contains the characteristic Y29 OηH signal. The direct involvement of the distal lysine in stabilizing exogenous cyanide therefore seems unlikely.

The ^{1}H–^{15}N HSQC data of wild-type rTHB1 reveal two NH_2 groups belonging to the major isomer and having ^{1}H signals at 11.11 and 5.27 ppm (^{15}N at 96.3 ppm) and 8.63 and −0.90 ppm (^{15}N at 103.3 ppm). The first of these NH_2 groups has NOEs to the rings of Phe28 and Tyr29 and is assigned to Gln54 (E11). The other is assigned to Gln50 (E7). A model of the distal hydrogen bond network to cyanide is illustrated in Figure S10A of the Supporting Information.

The sequence alignment of Figure 1A and analogy to the determined structures of cyanide-bound GlbN (PDB entry 4L2M) and CtrHb (PDB entry 1DLY) suggest that several residues should be in close contact with the heme group. Thus, an upfield-shifted valine with NOEs to the 3-CH_3, 4-vinyl Hβ_{cis}, and ring protons of Phe28 is assigned to Val94, in the G helix. Near the 1-CH_3 group, the signals of a Leu and a Phe ring belong to Leu73 and Phe57, respectively. In contact with the 2-vinyl, Phe, Val, and Ala side chains are detected and identified as Phe91, Phe28, Val94, Val119, and Ala122. Tyr68, along with Phe57 and Leu73, is in contact with the 8-CH_3 group, whereas the 5-CH_3 group has NOEs to Phe41 and Phe42. A representative set of NOEs is shown in Figure S11 of the Supporting Information. All assignments are consistent with the observed scalar connectivities and ^{1}H–^{15}N-based sequential assignments. A model of the proximal side of the heme is illustrated in Figure S10B of the Supporting Information.

An additional conserved feature of TrHb1s is the formation of a side chain–main chain hydrogen bond between a histidine at the beginning of the G helix (Nδ acceptor) and an amide in the turn preceding it (NH donor). In rTHB1, this helix capping interaction involves Asn87 NH and His90 Nδ1 and is in large part responsible for the downfield shift of Asn87 NH (major ^{1}H signal at 11.22 ppm; minor signal at 11.33 ppm). In the absence

dx.doi.org/10.1021/bi5005206 | *Biochemistry* 2014, 53, 4573–4589

of an exogenous ligand, these resonances remain downfield-shifted and are useful markers of the redox state of the protein as mentioned above. Protein chemical shifts are listed in Table S4 of the Supporting Information.

Overall, the spectroscopic results confirm that cyanomet rTHB1 resembles in fold and heme pocket geometry the related *Synechocystis* GlbN (PDB entry 1S69), *Synechococcus* GlbN (PDB entry 4L2M), *Mycobacterium tuberculosis* TrHbN (PDB entry 1RTE), *Tetrahymena pyriformis* trHb (PDB entry 3AQ5), and *C. eugametos* CtrHb (PDB entry 1DLY). The distal hydrogen bond network that stabilizes exogenous ligands is present. Despite the conserved fold and the conserved Tyr B10, however, the proteins are significantly different in the absence of an exogenous ligand. At neutral pH, bis-histidine coordination of the heme iron through His F8 (proximal) and His E10 is observed in ferric and ferrous GlbNs.[28,54,55] *M. tuberculosis* TrHbN and *T. pyriformis* trHb bind water in the ferric state (aquomet form) and become five-coordinate species upon being reduced to the ferrous state.[64,65] In *C. eugametos* CtrHb, Tyr B10 was proposed to be the sixth ligand to the iron,[52] and in *C. reinhardtii* THB1, the distal ligand is Lys E10. These different coordination modes are expected to condition heme reactivity.

The structure of THB1 in the absence of exogenous ligand remains to be fully elucidated. The resemblance to the bis-histidine GlbNs of Figure 1A is expected because of the common E10 ligation. In GlbNs, Tyr B10 is not in the heme pocket, which would explain the small effect of the Y29F replacement on the acid−base transition observed at pH 6.5 in rTHB1 (Figure S2 of the Supporting Information). This transition, attributed to the ionization equilibrium of Lys53, occurs ~3.5 pH units lower than for a solvent-exposed lysine and indicates a free energy expenditure on the order of 20 kJ/mol, similar to the cost of ligating the proximal histidine at pH 3[66] but to be compensated for at neutral pH.

rTHB1 Is Capable of Efficient NOD Activity. NOD activity is a common function of globins that is often imputed to TrHbs. For example, *M. tuberculosis* TrHbN[67] and *T. pyriformis* TrHb1[65] are both likely to serve in the capacity of $NO^{\bullet}$ detoxifiers. Although there are differences in the heme pockets of these proteins, they share the distal hydrogen bond network identified by NMR spectroscopy in cyanomet rTHB1. This network may enhance the superoxide character of the O_2-bound state and facilitate the NOD reaction. In the case of *C. reinhardtii*, NOD activity may be useful for protection from nitrosative damage and for the regulation of processes involving $NO^{\bullet}$.

To investigate the ability of rTHB1 to undergo multiple NOD turnovers, a simple *in vitro* assay was designed that utilizes the optical spectra shown in Figure 3 (see Materials and Methods). Figure 11A illustrates typical results. At time zero, a molar equivalent of MAHMA-NONOate was added to a sample containing rTHB1-O_2 and the Fd/$NADP^+$ reduction system. An immediate decrease in absorbance at 581 and 545 nm registers the disappearance of rTHB1-O_2. At the end of this rapid phase, the spectrum corresponds to a mixture of ferric rTHB1 and rTHB1-O_2 (66 and 34%, respectively, in this particular experiment). The protein then returns to 100% rTHB1-O_2 under the effect of the enzymatic reduction system and dissolved O_2. Under these conditions, conversion is observed from the ferric state directly to the oxy state without detection of a ferrous intermediate.

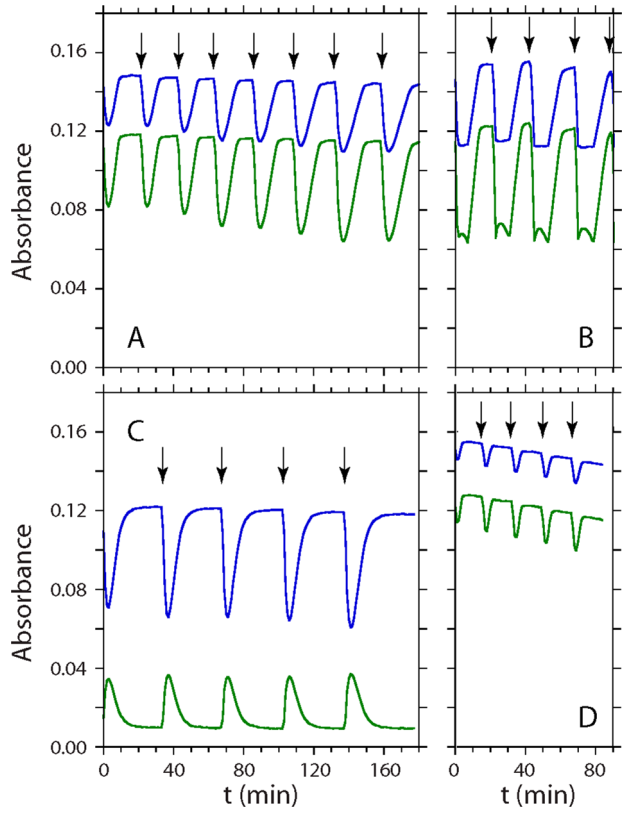

Figure 11. NOD activity of rTHB1. The traces illustrate the temporal changes in absorbance in the visible region. Samples contained ~10 μM protein in 100 mM phosphate buffer (pH 7.1) and a Fd/$NADP^+$ reduction system. (A) Time traces at 545 nm (top line, blue) and 581 nm (bottom line, green) upon repeated addition of 1 equiv of MAHMA-NONOate to wild-type rTHB1-O_2. The first addition occurred at time zero; subsequent additions are marked by vertical arrows. (B) Same as panel A, using 1.5 equiv of MAHMA-NONOate. The additional minor phase during the "turnover" period corresponds to buildup and decay of the ferric−nitrosyl adduct. (C) Time trace at 545 nm (blue) and 633 nm (green) upon repeated addition of 1 equiv of MAHMA-NONOate to K53A rTHB1-O_2. (D) Time trace at 545 nm (blue) and 581 nm (green) upon repeated addition of 1 equiv of MAHMA-NONOate to Y29F rTHB1-O_2.

Subsequent additions of MAHMA-NONOate lead to the same sawtooth behavior. The proportion of ferric state at the minimum of absorbance varies, with a tendency for an increase over the course of multiple $NO^{\bullet}$ injections. At concentrations of the $NO^{\bullet}$ donor capable of releasing 3 rather than 2 times the amount of protein, the ferric form binds $NO^{\bullet}$, giving rise to the altered profile shown in Figure 11B. At no point was the ferrous−nitrosyl adduct of rTHB1 detected. The same experiment conducted with horse skeletal muscle Mb gave the profile shown in Figure S12 of the Supporting Information.

To verify that rTHB1 turns over $NO^{\bullet}$ and forms nitrate, the end mixtures were subjected to the Griess assay.[37] The Griess assay depends on the reaction of sulfanilic acid with nitrite to form an activated diazonium salt, ultimately producing the detected azo dye. Under conditions of excess Griess reagents, colorimetric product formation reports on nitrite concentration. In the absence of rTHB1, oxidation of $NO^{\bullet}$ by O_2 generates detectable quantities of nitrite most likely through the $NO^{\bullet} + {}^1/_2O_2$ reaction.[68] In the presence of rTHB1, however, a negligible amount of nitrite is found in solution (Figure S13 of the Supporting Information). This indicates that an enzymatic

dx.doi.org/10.1021/bi5005206 | *Biochemistry* 2014, 53, 4573−4589

reaction consumes $NO^{\bullet}$ considerably faster than the enzyme-free processes. Addition of *A. niger* NR to convert nitrate to nitrite showed that in the rTHB1 sample, ~90% of $NO^{\bullet}$ released by MAHMA-NONOate was oxidized to nitrate. A comparable yield was obtained with Mb.

The minimal set of reactions in the NOD assay includes (1) release of $NO^{\bullet}$ by MAHMA-NONOate (first-order decay, measured independently), (2) reaction of $NO^{\bullet}$ with rTHB1-O_2 (eqs 2 and 3, considered irreversible), (3) reduction of ferric rTHB1 via reduced Fd, (4) Fd re-reduction, and (5) O_2 binding by ferrous rTHB1 (reversible, measured independently in the absence of $NO^{\bullet}$). Although accurate rate constants for NOD activity cannot be obtained with this assay, it is possible to test the plausibility of the mechanism by simulating the kinetic traces corresponding to each $NO^{\bullet}$ addition. Reproduction of the experimental data shown in Figure 11A can be achieved with a first phase dominated by the release of $NO^{\bullet}$ by MAHMA-NONOate and a second phase limited by the rate of reduction of Fd by the NADPH system. At higher $NO^{\bullet}$ concentrations (Figure 11B), reversible binding of $NO^{\bullet}$ to ferric rTHB1 must also be included to account for the additional spectral feature.

The simplest interpretation of the data is that rTHB1 can process $NO^{\bullet}$ efficiently in the test tube and that it undergoes no or little damage as it turns over the substrates. This supports the possibility that if O_2 and $NO^{\bullet}$ are simultaneously available to THB1 in the cell, NOD activity is likely. Multiple turnovers, however, require a reducing agent. Reductants such as NADPH and glutathione are not effective with the recombinant protein when used in reasonable concentrations (data not shown). The identity of the reducing agent in the cell, dedicated to THB1 or not, is not known.

The NOD assay was repeated with Y29F and K53A rTHB1. Qualitatively, the sawtooth pattern shown in Figure 11A is observed with both proteins (Figure 11C,D), and nitrate yields are comparable to those obtained with wild-type rTHB1 (Figure S13 of the Supporting Information). However, two differences are noted with the variants. First, the intensity of the Y29F rTHB1 spectrum decreases steadily throughout the experiment. We hypothesize as proposed by others[65] that Tyr B10 stabilizes bound dioxygen and that its replacement with a phenylalanine exacerbates competing processes such as autoxidation (i.e., superoxide release), ultimately leading to heme damage. Second, the proportion of ferric protein reached after addition of MAHMA-NONOate to K53A rTHB1-O_2 is higher than for the wild-type protein and Y29F variant, and the recovery to the oxy state is slower than for those two proteins. These observations are consistent with a coordinated Lys E10 facilitating electron transfer from the reducing system. We also expect Lys E10, once displaced from its axial position, to engage in a salt bridge with a heme propionate and modulate iron accessibility.

THB1 Levels Are Linked to the Nitrogen Source. To complement the structural and chemical data, we pursued the *in vivo* characterization of THB1. To this end, we generated an anti-THB1 polyclonal antiserum. In a previous study,[19] presence of THB1 was confirmed by the identification through mass spectrometry of two proteolytic fragments from the flagella of the *C. reinhardtii bbs4-1* mutant. One of the peptides corresponds to an N-terminal extension to the truncated globin domain and most of the short α helix. The N-terminal extension is only a few residues long (Figure 1A), and analysis of the THB1 sequence with PredAlgo,[69] a program designed to reveal protein subcellular localization in green algae, does not suggest targeting to a specific organelle of the cell. On the basis of evidence that the N-terminal extension is expressed and unlikely to be important for protein targeting, this region of the protein was chosen for anti-THB1 antibody production.

Polyclonal antibodies raised against the N-terminal proteolytic fragment (red sequence in Figure 1A) recognize rTHB1 (Figure 2B, lane 1) and a protein within whole cell extracts of *C. reinhardtii* at the molecular weight that corresponds to full-length THB1 (Figure 2B, lane 2). The purified polyclonal antibodies appear to be highly specific; the only other detected band gives a weak response at a molecular weight slightly below 40000, seen only after prolonged overexposure (data not shown).

Given the assumption that THB1 interacts in some form with $NO^{\bullet}$, the native function of THB1 may well be linked to cellular activity that either creates $NO^{\bullet}$ or is regulated by the molecule. Nitrogen metabolism is a potential target for THB1 as it is both regulated by $NO^{\bullet}$[17] and can produce $NO^{\bullet}$ through a low-efficiency side reaction of NR acting on nitrite.[70] Nitrogen usage in *C. reinhardtii* is complicated by the fact that not all laboratory strains metabolize nitrogen in the same way. Both CC-1690 and CC-125 are commonly used laboratory strains of *C. reinhardtii*; CC-1690 is assumed to be genetically identical to the original Sager 21 gr laboratory strain, but CC-125 carries mutations within both the *NIT1* and *NIT2* genes.[71] The *NIT1* gene encodes the only NR found within *C. reinhardtii*;[72] it is responsible for reducing nitrate to nitrite via an NADPH-dependent reaction. *NIT2* encodes a transcription factor required for expression of genes involved in nitrogen assimilation and is activated by nitrate.[73] A cell with nonfunctional copies of either *NIT1* or *NIT2* is thus prevented from utilizing nitrate as a source for nitrogen. Figure 12A shows immunodetection of THB1 in protein extracts from whole cells grown in Sager-Granick M medium. THB1 is found in strain CC-1690 but is not detected in strain CC-125. The *NIT1* and *NIT2* mutations in the CC-125 strain can be separated using strains CC-1086 (containing only a mutation to the *NIT2* gene) and CC-2453 (containing only a mutation to the *NIT1* gene). As seen in Figure 12A, only strains with functional versions of the *NIT2* gene express detectable levels of THB1 within the cell.

When nitrate is present in the growth medium, *NIT2* induces expression of the nitrate assimilation pathway. Sager-Granick M medium uses 3.75 mM ammonium nitrate as the nitrogen source (i.e., equal amounts of ammonium and nitrate). When the M medium is modified to contain 7.5 mM ammonium chloride or 7.5 mM potassium nitrate, the amount of THB1 within *C. reinhardtii* strain CC-1690 varies (Figure 12B). When nitrate is absent from the medium, there is a marked depletion of THB1 protein from the cell. When cells are grown in original M medium and then placed in medium with only ammonium as a nitrogen source, the level of THB1 gradually decreases over the course of 48 h (Figure S14A of the Supporting Information). Conversely, when cells are grown in the presence of ammonium as the sole nitrogen source and then switched into the original M medium, detectable levels of THB1 appear within 6 h (Figure S14B of the Supporting Information).

The transcriptional regulation of the *THB1* gene was followed using RNA isolated from these individual strains (Figure 12C). The level of gene expression for the *THB1* gene was undetectable when either strain CC-125 or CC-1086 was analyzed; however, both CC-1690 and CC-2453 (containing

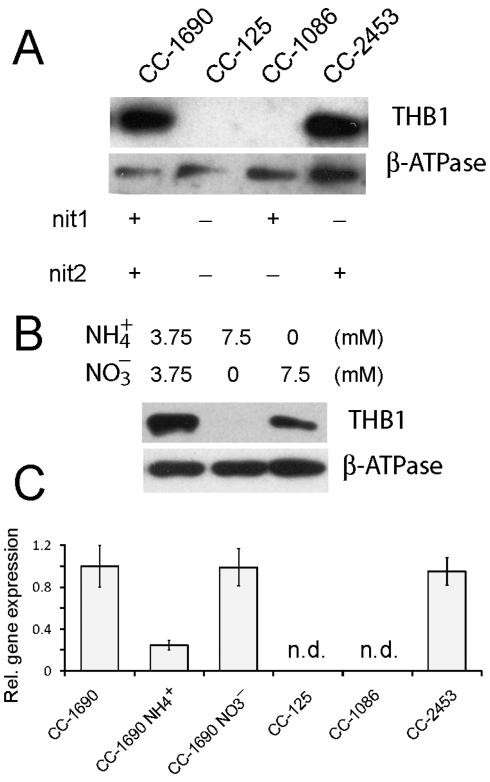

Figure 12. Variation in THB1 protein levels and *THB1* gene expression. (A) Western blot of whole cell extracts from *C. reinhardtii* strains CC-1690, CC-125, CC-1086, and CC-2453 probed with antibodies to THB1. All strains were grown in Sager-Granick M medium. The β subunit of the ATP synthase was used as a loading control. (B) Western blot of whole cell extracts probed with antibodies to THB1. Cells are from strain CC-1690 grown in Sager-Granick M medium with modifications to the nitrogen source in the media as indicated. The β subunit of the ATP synthase was used as a loading control. (C) Transcript abundances of *THB1* relative to *CBLP*, as determined by qPCR. Averages ± the standard deviation of three independent experiments performed on a mixture of biological duplicates are shown (nd, not detected). All samples were grown in Sager-Granick M medium except "NH_4^+" and "NO_3^-", which are strain CC-1690 grown in ammonium and nitrate, respectively, as in panel B.

functional *NIT2* genes) possessed equivalent levels of the transcript. The CC-1690 strain reduced its level of *THB1* transcripts when grown in a nitrate-free (7.5 mM ammonium) medium, in agreement with the depletion of the protein seen in the immunoblot (Figure 12A,B). In summary, these observations are consistent with induced expression of *THB1* being dependent on the presence of nitrate.

The Presence of THB1 in Flagella Is Not Related to Flagellar BBS4 Levels. A previous study reported that THB1 and three other proteins, all identified by mass spectrometric analysis of bands excised from an SDS–polyacrylamide gel, were greatly enriched in flagella of the nonphototactic mutant *bbs4-1* compared to its parent strain g1, which shows strong negative phototaxis.[19] The *bbs4-1* mutant was generated from strain g1 (*nit1*, *NIT2*) by insertional mutagenesis with a DNA fragment containing *NIT1* as the selectable marker;[74] the mutant is null for *BBS4*, which encodes a critical component of the BBSome, a multiprotein flagellar IFT cargo adapter.[19] The apparent accumulation of THB1 and the other proteins in the flagella of *bbs4-1* relative to the flagella of g1 raised the possibility that one or more of these proteins might be interfering with phototaxis. These results also led to the suggestion that these proteins are continuously cycling through the flagella and that their export from the flagella is dependent on the BBSome.

The availability of an antibody to THB1 and the finding that *THB1* expression could be regulated by the presence or absence of nitrate in the medium allowed us to reexamine the possibilities of a phototactic effect and a relation to the BBSome for THB1. To determine whether THB1 levels in the flagella are dependent on BBS4, we probed Western blots of isolated flagella from *bbs4-1* and g1 with anti-THB1. As previously reported,[19] THB1 was detected in the flagella of *bbs4-1* but not g1 cells (Figure S15A of the Supporting Information). Surprisingly, THB1 was also either not present or present at exceedingly low levels in g1 whole cells or cell bodies lacking flagella. THB1 transcripts also were not detected in g1, similar to strains carrying *nit2* mutations (Figure S15B of the Supporting Information). Although g1 was originally wild type for NIT2,[74] our current g1 strain failed to grow with either nitrate or nitrite as the sole nitrogen source; in contrast, *bbs4-1* was NIT2, as expected (Figure S15C of the Supporting Information). This suggests that the g1 strain maintained in the Witman lab and used in this study and that of Lechtreck et al.[19] is a *nit1 nit2* double mutant, most likely as a result of acquiring a spontaneous mutation in the *NIT2* gene some time during the dozen or so years between generation of the *bbs4-1* strain and the comparative analysis of the two strains by Lechtreck et al.[19] The results indicate that the differences in THB1 levels in flagella of g1 versus *bbs4-1* seen previously and again here simply reflect differences in THB1 expression. Importantly, flagella isolated from normally phototactic CC-1690 cells expressing both BBS4 and THB1 had levels of THB1 indistinguishable from that of *bbs4-1* flagella (Figure 13). Therefore, a lack of BBS4 does not lead to an accumulation of

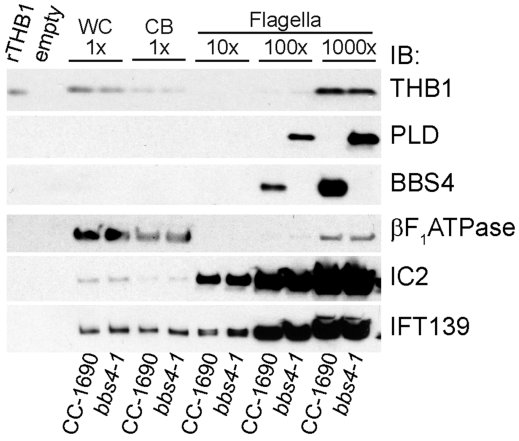

Figure 13. Test of the dependence of THB1 on BBS4 for flagellar export. Western blots of whole cells (WC), deflagellated cell bodies (CB), and isolated flagella from CC-1690 and *bbs4-1* were probed with the indicated antibodies (IB). Equivalent amounts of cells and cell bodies and a 10-, 100-, or 1000-fold excess of flagella were loaded (1× is 10^5 whole cells or cell bodies, 10× flagella is 2×10^6 flagella, etc.). The axonemal protein IC2 and the IFT protein IFT139 were used as loading controls. The β subunit of the ATP synthase was used to assess the possible level of cell body contamination of the isolated flagella. Flagellar levels of THB1, which are too high to be ascribed to cell body contamination, are equivalent in the presence (CC-1690) and absence (*bbs4-1*) of BBS4.

dx.doi.org/10.1021/bi5005206 | *Biochemistry* 2014, 53, 4573–4589

THB1 in flagella, and the presence of THB1 in flagella is unlikely to explain the phototaxis defect in *bbs4-1* cells.

Of the four proteins identified as being abnormally present in fractions of *bbs4-1* versus g1 flagella,[19] only THB1 was present in the aqueous phase enriched for flagellar matrix proteins; the rest, including phospholipase D (PLD), were present in the detergent phase enriched for membrane proteins. PLD has subsequently been shown to undergo a massive redistribution from the cell body to the flagella in the absence of BBS4; this redistribution is rapidly reversed when BBS4 is reintroduced into the flagella by fusing *bbs4-1* cells with wild-type cells.[23] The results of Figure 13 confirm that PLD accumulates in flagella of *bbs4-1* cells but not in flagella of wild-type cells, in this case strain CC-1690. Therefore, PLD does cycle through the flagella, and export of PLD from the flagella is dependent on the BBSome. Such BBSome-mediated export may be a feature of many membrane-associated proteins that undergo such cycling.[23] In contrast, because THB1 is a small soluble protein, it may diffuse freely through the barrier that separates the flagellar and cytosolic compartments; recent studies indicate that this barrier is permeable to soluble proteins of less than ~50 kDa.[75,76] Moreover, the fact that THB1 can enter the flagella strongly suggests that it is present in the cell cytoplasm and not strictly localized to a particular cell organelle. It may or may not have a specific function inside the flagellum.

Possible THB1 Function. Our results strongly suggest that the expression of the *THB1* gene is not constitutive but rather linked to the source of nitrogen available to the cell. This expression pattern also resembles that of NR, which is known to be under the control of the *NIT2* gene product.[72] A minimal interpretation of the data holds that THB1 and NR expressions are linked because THB1 is required to eliminate the $NO^{\bullet}$ released by NR. In addition to recycling the nitrogen to nitrate and lowering $NO^{\bullet}$ levels temporarily, THB1 could also temper S-nitrosylation and other RNS reactions. A similar mitigation role has been proposed for GlbN in *Synechococcus* sp. PCC 7002.[77] Like THB1, *Synechococcus* GlbN occurs at low levels in the cytoplasm, although unlike THB1, it is constitutively expressed. Challenging the *Synechococcus* cells with $NO^{\bullet}$ or a high concentration of nitrate reveals that GlbN protects against ROS and RNS.

With its structural plasticity, its ability to bind ligands, and its NOD activity, THB1 may participate in downstream regulatory processes. Recent studies have indeed found multiple NO-regulated pathways within *C. reinhardtii*, including copper stress response,[78] hypoxia,[18] and ammonium and nitrate transport.[17,79] $NO^{\bullet}$ regulation would not, however, be limited to THB1 because physiologic conditions exist under which exogenous $NO^{\bullet}$ is present while synthesis of THB1 is dramatically curtailed. Another agent, possibly one of the other many putative hemoglobins, would be needed to manage the $NO^{\bullet}$ load. In fact, potentially overlapping roles of all hemoglobins will complicate the identification of an unambiguous THB1 phenotype in future experiments with knock-down strains. The interrelation of $NO^{\bullet}$, RNS, and ROS chemistries in and out of the cell also presents special difficulties for the interpretation of results obtained under various challenges to cell growth.

Conclusion. We have shown that in THB1 the heme iron has two axial ligands: the proximal histidine in the F helix and a displaceable distal lysine (neutral Lys53) in the E helix. The structure of the His−Fe−Lys protein is expected to resemble that of GlbN in the bis-histidine state. The His−Fe−Lys scheme, like the His−Fe−His scheme, provides a means of enhancing electron transfer kinetics, affecting ligand association and dissociation rates, and influencing the reduction potential relative to a pentacoordinate counterpart. These effects can be harnessed to control NOD activity and other enzymatic reactions with requirements of redox cycling and substrate access and egress. *In vitro*, rTHB1 is an efficient $NO^{\bullet}$ dioxygenase, and the link to nitrogen metabolism, specifically expression of NR, suggests that a similar activity occurs in the cell. Further investigation will establish the distinct advantages and disadvantages of the His−Fe−Lys scheme under various cellular conditions of ROS load, RNS load, and pH.

Hemoglobins first appeared more than 3 billion years ago in a biosphere substantially different from ours. Without significant atmospheric oxygen and with a host of highly reduced molecules, stringent control of redox chemistry must have been essential to the earliest forms of life. Hbs have been retained since those early days and have remained within the genetic toolbox of organisms across the entire spectrum of life. Many of these Hbs have been proposed to function in roles related to reactive nitrogen usage.[13,80,81] *C. reinhardtii* is a well-studied model organism,[82−84] and exploring the function of TrHbs within this alga will harness a wealth of knowledge for defining the role of these proteins. The study of THB1 presented here constitutes a first step toward a comprehensive investigation of photosynthetic microbial Hbs.

■ ASSOCIATED CONTENT

Supporting Information

qPCR probes, ^{1}H chemical shifts of the heme group in ferrous Y29F rTHB1, ^{1}H chemical shifts of the axial lysine (K53) in ferrous Y29F rTHB1, ^{1}H chemical shifts and NOEs of selected heme pocket residues in cyanomet wild-type rTHB1, ^{1}H chemical shifts of the heme group in cyanomet Y29F rTHB1, ^{1}H chemical shifts and NOEs of selected heme pocket residues in cyanomet Y29F rTHB1, circular dichroism spectrum of ferric rTHB1, pH titration of ferric wild-type and Y29F rTHB1, optical spectrum of ferrous wild-type rTHB1 at three pH values, pH titration of ferric wild-type and K53A rTHB1, aromatic region of the $^{1}H-^{13}C$ HMQC spectrum of ferric wild-type and Y29F rTHB1, identification of the K53 $N\zeta H_2$ signal in ferrous wild-type rTHB1, ^{1}H signature of the heme vinyl groups in wild-type cyanomet rTHB1, diagram of intra-heme NOEs in wild-type cyanomet rTHB1, assignment of Phe28 and Tyr29 in wild-type cyanomet rTHB1, model of the heme pocket of cyanomet THB1, key heme pocket NOEs in cyanomet rTHB1, NOD assay of myoglobin, representative Griess assay results, THB1 levels over time as a function of nitrogen source, and determination of THB1 expression and Nit1 and Nit2 phenotypes for g1 and *bbs4-1*. This material is available free of charge via the Internet at http://pubs.acs.org.

■ AUTHOR INFORMATION

Corresponding Authors

*E-mail: lecomte_jtj@jhu.edu. Telephone: (410) 516-7019.

*E-mail: george.witman@umassmed.edu. Telephone: (508) 856-4038.

Funding

This work was supported by National Science Foundation Grants MCB-0843439 and MCB-1330488 to J.T.J.L., National Institutes of Health Grant GM030626 to G.B.W., and the Robert W. Booth Endowment at the University of

Massachusetts Medical School to G.B.W. D.B.N. was supported by National Institutes of Health Grant T32 GM080189. L.G. was supported by National Science Foundation Grant DBI-1262985.

Notes

The authors declare no competing financial interest.

■ ACKNOWLEDGMENTS

We thank Karen Beemon for assistance with the gene expression experiments, Katherine Tripp for assistance with CD data collection, and Ananya Majumdar for assistance with ESE experiments.

■ ABBREVIATIONS

1D, one-dimensional; 2D, two-dimensional; 3D, three-dimensional; BBS, Bardet-Biedl syndrome; CB, cell body; CtrHb, heme domain (residues 44−164) of *C. eugametos* LI637; DQF-COSY, double-quantum-filtered correlation spectroscopy; DT, sodium dithionite; ESE, electron self-exchange; ET, electron transfer; FAD, flavin adenine dinucleotide; Fd, spinach ferredoxin; GODCAT, glucose oxidase/catalase dioxygen scavenging system; GR, Griess reagents; Hb, hemoglobin; HMQC, heteronuclear multiple-quantum coherence; HSQC, heteronuclear single-quantum coherence; IFT, intraflagellar transport; MAHMA-NONOate, 6-(2-hydroxy-1-methyl-2-nitrosohydrazino)-*N*-methyl-1-hexanamine; Mb, myoglobin; NOD, nitric oxide dioxygenase; NOESY, nuclear Overhauser spectroscopy; NR, nitrate reductase; N_Z, longitudinal ^{15}N magnetization; PAGE, polyacrylamide gel electrophoresis; pH*, pH uncorrected for isotope effects; PLD, phospholipase D; RNS, reactive nitrogen species; ROS, reactive oxygen species; rTHB1, recombinant THB1; SDS, sodium dodecyl sulfate; TAP, tris acetate phosphate; TCEP, tris(2-carboxyethyl)-phosphine; THB1, product of the *THB1* gene of *C. reinhardtii*; TOCSY, total correlation spectroscopy; TE, Tris-EDTA; TrHb, truncated Hb; TrHb1, group I TrHb; WC, whole cell; ZZ, mixing of longitudinal magnetization.

■ REFERENCES

(1) Potts, M., Angeloni, S. V., Ebel, R. E., and Bassam, D. (1992) Myoglobin in a cyanobacterium. *Science 256*, 1690−1691.

(2) Wittenberg, J. B., Bolognesi, M., Wittenberg, B. A., and Guertin, M. (2002) Truncated hemoglobins: A new family of hemoglobins widely distributed in bacteria, unicellular eukaryotes and plants. *J. Biol. Chem. 277*, 871−874.

(3) Hill, D. R., Belbin, T. J., Thorsteinsson, M. V., Bassam, D., Brass, S., Ernst, A., Boger, P., Paerl, H., Mulligan, M. E., and Potts, M. (1996) GlbN (cyanoglobin) is a peripheral membrane protein that is restricted to certain *Nostoc* spp. *J. Bacteriol. 178*, 6587−6598.

(4) Couture, M., Chamberland, H., St-Pierre, B., Lafontaine, J., and Guertin, M. (1994) Nuclear genes encoding chloroplast hemoglobins in the unicellular green alga *Chlamydomonas eugametos*. *Mol. Gen. Genet. 243*, 185−197.

(5) Pesce, A., Couture, M., Dewilde, S., Guertin, M., Yamauchi, K., Ascenzi, P., Moens, L., and Bolognesi, M. (2000) A novel two-over-two α-helical sandwich fold is characteristic of the truncated hemoglobin family. *EMBO J. 19*, 2424−2434.

(6) Couture, M., and Guertin, M. (1996) Purification and spectroscopic characterization of a recombinant chloroplastic hemoglobin from the green unicellular alga *Chlamydomonas eugametos*. *Eur. J. Biochem. 242*, 779−787.

(7) Vinogradov, S. N., Hoogewijs, D., Bailly, X., Arredondo-Peter, R., Gough, J., Dewilde, S., Moens, L., and Vanfleteren, J. R. (2006) A phylogenomic profile of globins. *BMC Evol. Biol. 6*, 31.

(8) Vinogradov, S. N., Tinajero-Trejo, M., Poole, R. K., and Hoogewijs, D. (2013) Bacterial and archaeal globins: A revised perspective. *Biochim. Biophys. Acta 1834*, 1789−1800.

(9) Vazquez-Limon, C., Hoogewijs, D., Vinogradov, S. N., and Arredondo-Peter, R. (2012) The evolution of land plant hemoglobins. *Plant Sci. 191*, 71−81.

(10) Anbar, A. D. (2008) Elements and evolution. *Science 322*, 1481−1483.

(11) Crowe, S. A., Dossing, L. N., Beukes, N. J., Bau, M., Kruger, S. J., Frei, R., and Canfield, D. E. (2013) Atmospheric oxygenation three billion years ago. *Nature 501*, 535−538.

(12) Gardner, P. R. (2005) Nitric oxide dioxygenase function and mechanism of flavohemoglobin, hemoglobin, myoglobin and their associated reductases. *J. Inorg. Biochem. 99*, 247−266.

(13) Gardner, P. R. (2012) Hemoglobin, a nitric-oxide dioxygenase. *Scientifica 2012*, 683729.

(14) De Marinis, E., Casella, L., Ciaccio, C., Coletta, M., Visca, P., and Ascenzi, P. (2009) Catalytic peroxidation of nitrogen monoxide and peroxynitrite by globins. *IUBMB Life 61*, 62−73.

(15) Bowman, L. A., McLean, S., Poole, R. K., and Fukuto, J. M. (2011) The diversity of microbial responses to nitric oxide and agents of nitrosative stress close cousins but not identical twins. *Adv. Microb. Physiol. 59*, 135−219.

(16) Gardner, P. R., Gardner, A. M., Martin, L. A., and Salzman, A. L. (1998) Nitric oxide dioxygenase: An enzymic function for flavohemoglobin. *Proc. Natl. Acad. Sci. U.S.A. 95*, 10378−10383.

(17) Sanz-Luque, E., Ocana-Calahorro, F., Llamas, A., Galvan, A., and Fernandez, E. (2013) Nitric oxide controls nitrate and ammonium assimilation in *Chlamydomonas reinhardtii*. *J. Exp. Bot. 64*, 3373−3383.

(18) Hemschemeier, A., Duner, M., Casero, D., Merchant, S. S., Winkler, M., and Happe, T. (2013) Hypoxic survival requires a 2-on-2 hemoglobin in a process involving nitric oxide. *Proc. Natl. Acad. Sci. U.S.A. 110*, 10854−10859.

(19) Lechtreck, K. F., Johnson, E. C., Sakai, T., Cochran, D., Ballif, B. A., Rush, J., Pazour, G. J., Ikebe, M., and Witman, G. B. (2009) The *Chlamydomonas reinhardtii* BBSome is an IFT cargo required for export of specific signaling proteins from flagella. *J. Cell Biol. 187*, 1117−1132.

(20) Johnson, E. A., and Lecomte, J. T. (2013) The globins of cyanobacteria and algae. *Adv. Microb. Physiol. 63*, 195−272.

(21) Witman, G. B. (1986) Isolation of *Chlamydomonas* flagella and flagellar axonemes. *Methods Enzymol. 134*, 280−290.

(22) Craige, B., Brown, J. M., and Witman, G. B. (2013) Isolation of *Chlamydomonas* flagella. *Current Protocols in Cell Biology 59*, 3.41.41−43.41.49.

(23) Lechtreck, K. F., Brown, J. M., Sampaio, J. L., Craft, J. M., Shevchenko, A., Evans, J. E., and Witman, G. B. (2013) Cycling of the signaling protein phospholipase D through cilia requires the BBSome only for the export phase. *J. Cell Biol. 201*, 249−261.

(24) Atteia, A., van Lis, R., Gelius-Dietrich, G., Adrait, A., Garin, J., Joyard, J., Rolland, N., and Martin, W. (2006) Pyruvate formate-lyase and a novel route of eukaryotic ATP synthesis in *Chlamydomonas* mitochondria. *J. Biol. Chem. 281*, 9909−9918.

(25) King, S. M., and Witman, G. B. (1990) Localization of an intermediate chain of outer arm dynein by immunoelectron microscopy. *J. Biol. Chem. 265*, 19807−19811.

(26) Cole, D. G., Diener, D. R., Himelblau, A. L., Beech, P. L., Fuster, J. C., and Rosenbaum, J. L. (1998) *Chlamydomonas* kinesin-II-dependent intraflagellar transport (IFT): IFT particles contain proteins required for ciliary assembly in *Caenorhabditis elegans* sensory neurons. *J. Cell Biol. 141*, 993−1008.

(27) Chang, C. W., Moseley, J. L., Wykoff, D., and Grossman, A. R. (2005) The LPB1 gene is important for acclimation of *Chlamydomonas reinhardtii* to phosphorus and sulfur deprivation. *Plant Physiol. 138*, 319−329.

(28) Scott, N. L., and Lecomte, J. T. J. (2000) Cloning, expression, purification, and preliminary characterization of a putative hemoglobin from the cyanobacterium *Synechocystis* sp. PCC 6803. *Protein Sci. 9*, 587−597.

(29) de Duve, C. (1948) A spectrophotometric method for the simultaneous determination of myoglobin and hemoglobin in extracts of human muscle. *Acta Chem. Scand. 2*, 264−289.
(30) Preimesberger, M. R., Wenke, B. B., Gilevicius, L., Pond, M. P., and Lecomte, J. T. J. (2013) Facile heme vinyl posttranslational modification in a hemoglobin. *Biochemistry 52*, 3478−3488.
(31) Gasteiger, E., Hoogland, C., Gattiker, A., Duvaud, S., Wilkins, M. R., Appel, R. D., and Bairoch, A. (2005) Protein Identification and Analysis Tools on the ExPASy Server. In *The Proteomics Protocols Handbook* (Walker, J. M., Ed.) Humana Press, Totowa, NJ.
(32) Englander, S. W., Calhoun, D. B., and Englander, J. J. (1987) Biochemistry without oxygen. *Anal. Biochem. 161*, 300−306.
(33) Hayashi, A., Suzuki, T., and Shin, M. (1973) An enzymic reduction system for metmyoglobin and methemoglobin, and its application to functional studies of oxygen carriers. *Biochim. Biophys. Acta 310*, 309−316.
(34) Hendler, R. W., and Shrager, R. I. (1994) Deconvolutions based on singular value decomposition and the pseudoinverse: A guide for beginners. *J. Biochem. Biophys. Methods 28*, 1−33.
(35) Bilsel, O., Zitzewitz, J. A., Bowers, K. E., and Matthews, C. R. (1999) Folding mechanism of the α-subunit of tryptophan synthase, an α/β barrel protein: Global analysis highlights the interconversion of multiple native, intermediate, and unfolded forms through parallel channels. *Biochemistry 38*, 1018−1029.
(36) Hrabie, J. A., Klose, J. R., Wink, D. A., and Keefer, L. K. (1993) New nitric oxide-releasing zwitterions derived from polyamines. *J. Org. Chem. 58*, 1472−1476.
(37) Griess, P. (1879) Bemerkungen zu der Abhandlung der HH Weselsky und Benedikt "Über einige Azoverbindungen". *Chem. Ber. 12*, 426−428.
(38) Verdon, C. P., Burton, B. A., and Prior, R. L. (1995) Sample pretreatment with nitrate reductase and glucose-6-phosphate dehydrogenase quantitatively reduces nitrate while avoiding interference by $NADP^+$ when the Griess reaction is used to assay for nitrite. *Anal. Biochem. 224*, 502−508.
(39) Johnson, K. A. (2009) Fitting enzyme kinetic data with KinTek Global Kinetic Explorer. *Methods Enzymol. 467*, 601−626.
(40) Wishart, D. S., Bigam, C. G., Yao, J., Abildgaard, F., Dyson, H. J., Oldfield, E., Markley, J. L., and Sykes, B. D. (1995) ^1H, ^{13}C and ^{15}N chemical shift referencing in biomolecular NMR. *J. Biomol. NMR 6*, 135−140.
(41) Delaglio, F., Grzesiek, S., Vuister, G. W., Zhu, G., Pfeifer, J., and Bax, A. (1995) NMRPipe: A multidimensional spectral processing system based on UNIX pipes. *J. Biomol. NMR 6*, 277−293.
(42) Goddard, T. D., and Kneller, D. G. (2006) *SPARKY 3*, University of California, San Francisco.
(43) Lecomte, J. T. J., Vu, B. C., and Falzone, C. J. (2005) Structural and dynamic properties of *Synechocystis* sp. PCC 6803 Hb revealed by reconstitution with Zn-protoporphyrin IX. *J. Inorg. Biochem. 99*, 1585−1592.
(44) Preimesberger, M. R., Pond, M. P., Majumdar, A., and Lecomte, J. T. J. (2012) Electron self-exchange and self-amplified posttranslational modification in the hemoglobins from *Synechocystis* sp. PCC 6803 and *Synechococcus* sp. PCC 7002. *JBIC, J. Biol. Inorg. Chem. 17*, 599−609.
(45) Cavanagh, J., Fairbrother, W. J., Palmer, A. G. I., and Skelton, N. J. (1996) *Protein NMR Spectroscopy. Principles and Practice*, Academic Press, San Diego.
(46) Vu, B. C., Jones, A. D., and Lecomte, J. T. J. (2002) Novel histidine-heme covalent linkage in a hemoglobin. *J. Am. Chem. Soc. 124*, 8544−8545.
(47) Falzone, C. J., and Lecomte, J. T. J. (2002) Assignment of the ^1H, ^{13}C, and ^{15}N signals of *Synechocystis* sp. PCC 6803 methemoglobin. *J. Biomol. NMR 23*, 71−72.
(48) Pond, M. P., Vuletich, D. A., Falzone, C. J., Majumdar, A., and Lecomte, J. T. J. (2009) ^1H, ^{15}N, and ^{13}C resonance assignments of the 2/2 hemoglobin from the cyanobacterium *Synechococcus* sp. PCC 7002 in the ferric bis-histidine state. *Biomol. NMR Assignments 3*, 211−214.
(49) Arnold, K., Bordoli, L., Kopp, J., and Schwede, T. (2006) The SWISS-MODEL workspace: A web-based environment for protein structure homology modelling. *Bioinformatics 22*, 195−201.
(50) Antonini, E., and Brunori, M. (1971) *Hemoglobin and myoglobin in their reactions with ligands*, Vol. *12*, North-Holland, Amsterdam.
(51) Bogumil, R., Maurus, R., Hildebrand, D. P., Brayer, G. D., and Mauk, A. G. (1995) Origin of the pH-dependent spectroscopic properties of pentacoordinate metmyoglobin variants. *Biochemistry 34*, 10483−10490.
(52) Das, T. K., Couture, M., Lee, H. C., Peisach, J., Rousseau, D. L., Wittenberg, B. A., Wittenberg, J. B., and Guertin, M. (1999) Identification of the ligands to the ferric heme of *Chlamydomonas* chloroplast hemoglobin: Evidence for ligation of tyrosine-63 (B10) to the heme. *Biochemistry 38*, 15360−15368.
(53) Couture, M., Das, T. K., Lee, H. C., Peisach, J., Rousseau, D. L., Wittenberg, B. A., Wittenberg, J. B., and Guertin, M. (1999) *Chlamydomonas* chloroplast ferrous hemoglobin. Heme pocket structure and reactions with ligands. *J. Biol. Chem. 274*, 6898−6910.
(54) Couture, M., Das, T. K., Savard, P. Y., Ouellet, Y., Wittenberg, J. B., Wittenberg, B. A., Rousseau, D. L., and Guertin, M. (2000) Structural investigations of the hemoglobin of the cyanobacterium *Synechocystis* PCC 6803 reveal a unique distal heme pocket. *Eur. J. Biochem. 267*, 4770−4780.
(55) Scott, N. L., Falzone, C. J., Vuletich, D. A., Zhao, J., Bryant, D. A., and Lecomte, J. T. J. (2002) The hemoglobin of the cyanobacterium *Synechococcus* sp. PCC 7002: Evidence for hexacoordination and covalent adduct formation in the ferric recombinant protein. *Biochemistry 41*, 6902−6910.
(56) Patel, N., Seward, H. E., Svensson, A., Gurman, S. J., Thomson, A. J., and Raven, E. L. (2003) Exploiting the conformational flexibility of leghemoglobin: A framework for examination of heme protein axial ligation. *Arch. Biochem. Biophys. 418*, 197−204.
(57) Ubbink, M., Campos, A. P., Teixeira, M., Hunt, N. I., Hill, H. A., and Canters, G. W. (1994) Characterization of mutant Met100Lys of cytochrome *c*-550 from *Thiobacillus versutus* with lysine-histidine heme ligation. *Biochemistry 33*, 10051−10059.
(58) Du, J., Perera, R., and Dawson, J. H. (2011) Alkylamine-ligated H93G myoglobin cavity mutant: A model system for endogenous lysine and terminal amine ligation in heme proteins such as nitrite reductase and cytochrome *f*. *Inorg. Chem. 50*, 1242−1249.
(59) La Mar, G. N., Satterlee, J. D., and de Ropp, J. S. (2000) Nuclear magnetic resonance of hemoproteins. In *The Porphyrin Handbook* (Smith, K. M., Kadish, K., and Guilard, R., Eds.) pp 185−298, Academic Press, Burlington, MA.
(60) Jeener, J., Meier, B. H., Bachmann, P., and Ernst, R. R. (1979) Investigation of exchange processes by two-dimensional NMR spectroscopy. *J. Chem. Phys. 71*, 4546−4553.
(61) Simonneaux, G., and Bondon, A. (2005) Mechanism of electron transfer in heme proteins and models: the NMR approach. *Chem. Rev. 105*, 2627−2646.
(62) Vu, B. C., Nothnagel, H. J., Vuletich, D. A., Falzone, C. J., and Lecomte, J. T. J. (2004) Cyanide binding to hexacoordinate cyanobacterial hemoglobins: Hydrogen bonding network and heme pocket rearrangement in ferric H117A *Synechocystis* Hb. *Biochemistry 43*, 12622−12633.
(63) Dellarole, M., Roumestand, C., Royer, C., and Lecomte, J. T. J. (2013) Volumetric properties underlying ligand binding in a monomeric hemoglobin: A high-pressure NMR study. *Biochim. Biophys. Acta 1834*, 1910−1922.
(64) Couture, M., Yeh, S. R., Wittenberg, B. A., Wittenberg, J. B., Ouellet, Y., Rousseau, D. L., and Guertin, M. (1999) A cooperative oxygen-binding hemoglobin from *Mycobacterium tuberculosis*. *Proc. Natl. Acad. Sci. U.S.A. 96*, 11223−11228.
(65) Igarashi, J., Kobayashi, K., and Matsuoka, A. (2011) A hydrogen-bonding network formed by the B10-E7-E11 residues of a truncated hemoglobin from *Tetrahymena pyriformis* is critical for stability of bound oxygen and nitric oxide detoxification. *JBIC, J. Biol. Inorg. Chem. 16*, 599−609.

(66) Hargrove, M. S., Barrick, D., and Olson, J. S. (1996) The association rate constant for heme binding to globin is independent of protein structure. *Biochemistry 35*, 11293−11299.
(67) Ouellet, H., Ouellet, Y., Richard, C., Labarre, M., Wittenberg, B., Wittenberg, J., and Guertin, M. (2002) Truncated hemoglobin HbN protects *Mycobacterium bovis* from nitric oxide. *Proc. Natl. Acad. Sci. U.S.A. 99*, 5902−5907.
(68) Ignarro, L. J., Fukuto, J. M., Griscavage, J. M., Rogers, N. E., and Byrns, R. E. (1993) Oxidation of nitric oxide in aqueous solution to nitrite but not nitrate: Comparison with enzymatically formed nitric oxide from L-arginine. *Proc. Natl. Acad. Sci. U.S.A. 90*, 8103−8107.
(69) Tardif, M., Atteia, A., Specht, M., Cogne, G., Rolland, N., Brugiere, S., Hippler, M., Ferro, M., Bruley, C., Peltier, G., Vallon, O., and Cournac, L. (2012) PredAlgo: A new subcellular localization prediction tool dedicated to green algae. *Mol. Biol. Evol. 29*, 3625−3639.
(70) Sakihama, Y., Nakamura, S., and Yamasaki, H. (2002) Nitric oxide production mediated by nitrate reductase in the green alga *Chlamydomonas reinhardtii*: An alternative NO production pathway in photosynthetic organisms. *Plant Cell Physiol. 43*, 290−297.
(71) Kubo, T., Abe, J., Saito, T., and Matsuda, Y. (2002) Genealogical relationships among laboratory strains of *Chlamydomonas reinhardtii* as inferred from matrix metalloprotease genes. *Curr. Genet. 41*, 115−122.
(72) Fernandez, E., Schnell, R., Ranum, L. P., Hussey, S. C., Silflow, C. D., and Lefebvre, P. A. (1989) Isolation and characterization of the nitrate reductase structural gene of *Chlamydomonas reinhardtii*. *Proc. Natl. Acad. Sci. U.S.A. 86*, 6449−6453.
(73) Camargo, A., Llamas, A., Schnell, R. A., Higuera, J. J., Gonzalez-Ballester, D., Lefebvre, P. A., Fernandez, E., and Galvan, A. (2007) Nitrate signaling by the regulatory gene NIT2 in *Chlamydomonas*. *Plant Cell 19*, 3491−3503.
(74) Pazour, G. J., Sineshchekov, O. A., and Witman, G. B. (1995) Mutational analysis of the phototransduction pathway of *Chlamydomonas reinhardtii*. *J. Cell Biol. 131*, 427−440.
(75) Kee, H. L., Dishinger, J. F., Blasius, T. L., Liu, C. J., Margolis, B., and Verhey, K. J. (2012) A size-exclusion permeability barrier and nucleoporins characterize a ciliary pore complex that regulates transport into cilia. *Nat. Cell Biol. 14*, 431−437.
(76) Breslow, D. K., Koslover, E. F., Seydel, F., Spakowitz, A. J., and Nachury, M. V. (2013) An in vitro assay for entry into cilia reveals unique properties of the soluble diffusion barrier. *J. Cell Biol. 203*, 129−147.
(77) Scott, N. L., Xu, Y., Shen, G., Vuletich, D. A., Falzone, C. J., Li, Z., Ludwig, M., Pond, M. P., Preimesberger, M. R., Bryant, D. A., and Lecomte, J. T. J. (2010) Functional and structural characterization of the 2/2 hemoglobin from *Synechococcus* sp. PCC 7002. *Biochemistry 49*, 7000−7011.
(78) Zhang, L. P., Mehta, S. K., Liu, Z. P., and Yang, Z. M. (2008) Copper-induced proline synthesis is associated with nitric oxide generation in *Chlamydomonas reinhardtii*. *Plant Cell Physiol. 49*, 411−419.
(79) de Montaigu, A., Sanz-Luque, E., Galvan, A., and Fernandez, E. (2010) A soluble guanylate cyclase mediates negative signaling by ammonium on expression of nitrate reductase in *Chlamydomonas*. *Plant Cell 22*, 1532−1548.
(80) Perazzolli, M., Romero-Puertas, M. C., and Delledonne, M. (2006) Modulation of nitric oxide bioactivity by plant haemoglobins. *J. Exp. Bot. 57*, 479−488.
(81) Reeder, B. J. (2010) The redox activity of hemoglobins: From physiologic functions to pathologic mechanisms. *Antioxid. Redox Signaling 13*, 1087−1123.
(82) Harris, E. H. (2001) *Chlamydomonas* as a model organism. *Annu. Rev. Plant Physiol. 52*, 363−406.
(83) Merchant, S. S., Prochnik, S. E., Vallon, O., Harris, E. H., Karpowicz, S. J., Witman, G. B., Terry, A., Salamov, A., Fritz-Laylin, L. K., Marechal-Drouard, L., Marshall, W. F., Qu, L. H., Nelson, D. R., Sanderfoot, A. A., Spalding, M. H., Kapitonov, V. V., Ren, Q., Ferris, P., Lindquist, E., Shapiro, H., Lucas, S. M., Grimwood, J., Schmutz, J., Cardol, P., Cerutti, H., Chanfreau, G., Chen, C. L., Cognat, V., Croft, M. T., Dent, R., Dutcher, S., Fernandez, E., Fukuzawa, H., Gonzalez-Ballester, D., Gonzalez-Halphen, D., Hallmann, A., Hanikenne, M., Hippler, M., Inwood, W., Jabbari, K., Kalanon, M., Kuras, R., Lefebvre, P. A., Lemaire, S. D., Lobanov, A. V., Lohr, M., Manuell, A., Meier, I., Mets, L., Mittag, M., Mittelmeier, T., Moroney, J. V., Moseley, J., Napoli, C., Nedelcu, A. M., Niyogi, K., Novoselov, S. V., Paulsen, I. T., Pazour, G., Purton, S., Ral, J. P., Riano-Pachon, D. M., Riekhof, W., Rymarquis, L., Schroda, M., Stern, D., Umen, J., Willows, R., Wilson, N., Zimmer, S. L., Allmer, J., Balk, J., Bisova, K., Chen, C. J., Elias, M., Gendler, K., Hauser, C., Lamb, M. R., Ledford, H., Long, J. C., Minagawa, J., Page, M. D., Pan, J., Pootakham, W., Roje, S., Rose, A., Stahlberg, E., Terauchi, A. M., Yang, P., Ball, S., Bowler, C., Dieckmann, C. L., Gladyshev, V. N., Green, P., Jorgensen, R., Mayfield, S., Mueller-Roeber, B., Rajamani, S., Sayre, R. T., Brokstein, P., Dubchak, I., Goodstein, D., Hornick, L., Huang, Y. W., Jhaveri, J., Luo, Y., Martinez, D., Ngau, W. C., Otillar, B., Poliakov, A., Porter, A., Szajkowski, L., Werner, G., Zhou, K., Grigoriev, I. V., Rokhsar, D. S., and Grossman, A. R. (2007) The *Chlamydomonas* genome reveals the evolution of key animal and plant functions. *Science 318*, 245−250.
(84) Terashima, M., Specht, M., and Hippler, M. (2011) The chloroplast proteome: A survey from the *Chlamydomonas reinhardtii* perspective with a focus on distinctive features. *Curr. Genet. 57*, 151−168.

NOTE ADDED AFTER ASAP PUBLICATION

This paper was published ASAP on July 9, 2014. Due to production error, it was published with an error in equation 1. The corrected version was reposted on July 22, 2014.